THE DYNAMIC STRESS-STRAIN RELATION OF ANNEALED 2S ALUMINUM UNDER COMPRESSION IMPACT

Thesis by

James Edgar Johnson

In Partial Fulfillment of the Requirements

for the Degree of

Doctor of Philosophy

California Institute of Technology

Pasadena, California

1953

ACKNOWLEDGMENTS

The author wishes to express his deep feeling of gratitude to Professors D. S. Clark and D. S. Wood, who directed this research, and whose unfailing interest and help made this research possible.

The testing program was conducted under the sponsorship of the Office of Naval Research. The author also expresses his appreciation to this agency for their support of the work.

ABSTRACT

This thesis presents the results of a study of the stress-strain relation of a metal when subjected to compression impact. An annealed 2S aluminum is used for this investigation. Two methods of securing the dynamic stress-strain curve are considered; namely, from the measurement of impact stress and of maximum plastic strain as functions of the impact velocity from 3.15 to 125 ft/sec. The dynamic stress-strain relations obtained by these methods are compared with the static stress-strain curve. Both of the dynamic stress-strain relations lie considerably above the static curve. However, the two dynamic relations are not coincident which indicates that a single dynamic stress-strain curve cannot properly describe the behavior of the material for all impact velocities. A family of stress-strain curves is postulated in order to explain the difference between these two relations. Each curve of the family depends upon the final strain or impact velocity.

It is further concluded that the rise of the stress-strain curve under dynamic loading cannot be induced by moderate loading rates.

TABLE OF CONTENTS

LIST OF TABLES

LIST OF FIGURES

LIST OF FIGURES CONT'D

INTRODUCTION

The behavior of metals and alloys under dynamic conditions has received considerable attention in recent years (1-6)*. It is found that in the plastic range, the stress for a given strain is increased when the rate of loading is increased. This effect is particularly noticed in high speed impact tests where the rate of loading and deformation are very high. Taylor and Whiffin (7-8) have found that the yield stress of steel in high speed impact tests is considerably higher than the static yield stress. The strength of annealed copper under impact conditions is also increased above the static value. In compression impact tests on annealed copper, Habib (9) has shown that under impact conditions, the stress for a given strain is somewhat greater than the static stress at the same strain. The results of an investigation by Clark and Wood (10) on a large number of metals and alloys indicates that the ultimate tensile strength of all the materials tested is greater under dynamic conditions than under static conditions.

However, the results of these tests are questionable since the stress-strain relations and maximum stresses

---

* Figures appearing in parenthesis refer to the references listed at the end of this thesis.

are deduced from measurements made on the specimen as a whole. It has been shown by Lee and Wolf (11) that a material test performed at high speed may be markedly influenced by plastic wave propagation effects. The stress-strain relation under these conditions cannot be deduced from measurements made on the specimen as a whole since a variation of strain occurs along the specimen.

Rapid load tension and compression impact tests have been performed on annealed low carbon steel (12-13) which exhibits a well defined upper yield stress. The test specimen used in the rapid load tension tests is short enough and the rate of rise of stress low enough so that no appreciable stress waves occur in the specimen. The strain propagation effects were considered in the compression impact tests. The results show that the material can withstand a stress up to twice the static upper yield stress for short periods of time before plastic deformation is initiated.

However, comparatively few tests have been performed in which the stress-strain relation under dynamic loading is determined. Kolsky (14) has performed tests on copper and lead in which the stress-strain relation under very high rates of loading was determined. A thin section of the material was placed between two sections of a Hopkinson pressure bar. The test material was plastically deformed

when a compression wave due to the detonation of an explosive charge at one end of the pressure bar was propagated through the bars and specimen. The particle velocity of each bar section was measured as a function of time during impact. The stress-strain curve was then calculated from the particle velocity measurements. The results indicate that the stress for a given strain at very high loading rates is equal to about twice the stress under static conditions. However, it is difficult to interpret the results of this investigation since the yielding condition of the material is affected by the large component of stress in the radial direction induced by the plane strain of the material.

An experimental technique has now been developed in the Dynamic Properties Laboratory of the California Institute of Technology to determine the stress-strain relation of a material under impact conditions. The technique used to accomplish this is as follows: a compression stress is applied to one end of a long cylindrical specimen by longitudinal impact with an anvil bar which remains elastic during the test. The stress-time relation at the impact end of the specimen, the strain-time relation at various positions along the specimen, and the plastic strain distribution in the specimen can be determined. The stress-strain relation of the material under compression impact can be deduced from these measurements. The theory of plastic

wave propagation in long thin bars developed by von Karman (15-16) can be used to describe the deformation in the spec during impact. Reflections of the waves from the free end of the specimen and interface between the anvil bar and specimen can be readily determined.

The purpose of this investigation is to obtain experimental data which will aid in determining the stress-strain relation of annealed 2S aluminum under impact conditions. The method used is to determine the stress at the impact end of the specimen and the residual strain in the specimen as a function of impact velocity. The dynamic stress-strain curve is then deduced from these measurements by the use of the theory of plastic wave propagation.

A further purpose of this investigation is to determine if the strain deduced from initial stress-impact velocity measurements is equal to the strain measured after impact. The stress-strain relation associated with the initial impact load may not continue to represent the behavior of the material for an indefinite time and an additional strain may result from relaxation of the material.

EQUIPMENT

Vertical Impact Machine:

The compression impact tests were made with the vertical impact machine shown in Fig. 1. A guard tube shown in Fig. 2 is held vertically in a central position between the rails of the machine by means of an expendable spacer. A stationary tobin bronze anvil bar of the same diameter as the specimen is centrally located within the guard tube by means of two sleeves. An expendable annealed copper cylinder is positioned between the lower end of the anvil bar and the fixed base. The copper cylinder serves to absorb most of the impact energy in the anvil bar by plastic deformation. Since some missalignment between the anvil bar and the specimen will occur, the top end of the anvil bar is provided with a 19 inch radius convex spherical surface to prevent initial impact with the corner of the specimen.

When the specimen impacts the stationary anvil bar a series of compression strains are propagated through the specimen and an elastic compression wave is propagated through the anvil bar. The yield strength of the anvil bar is higher than the stress imposed by the impact and, therefore, the bar behaves elastically during the test. Thus, any change

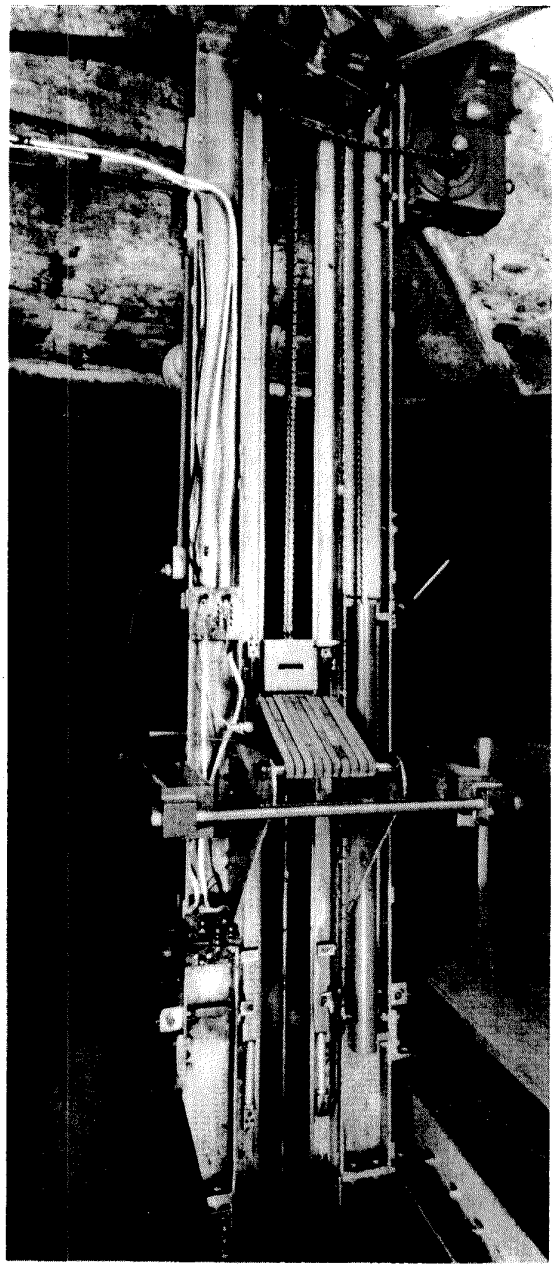

Fig. 1 Vertical Impact Machine.

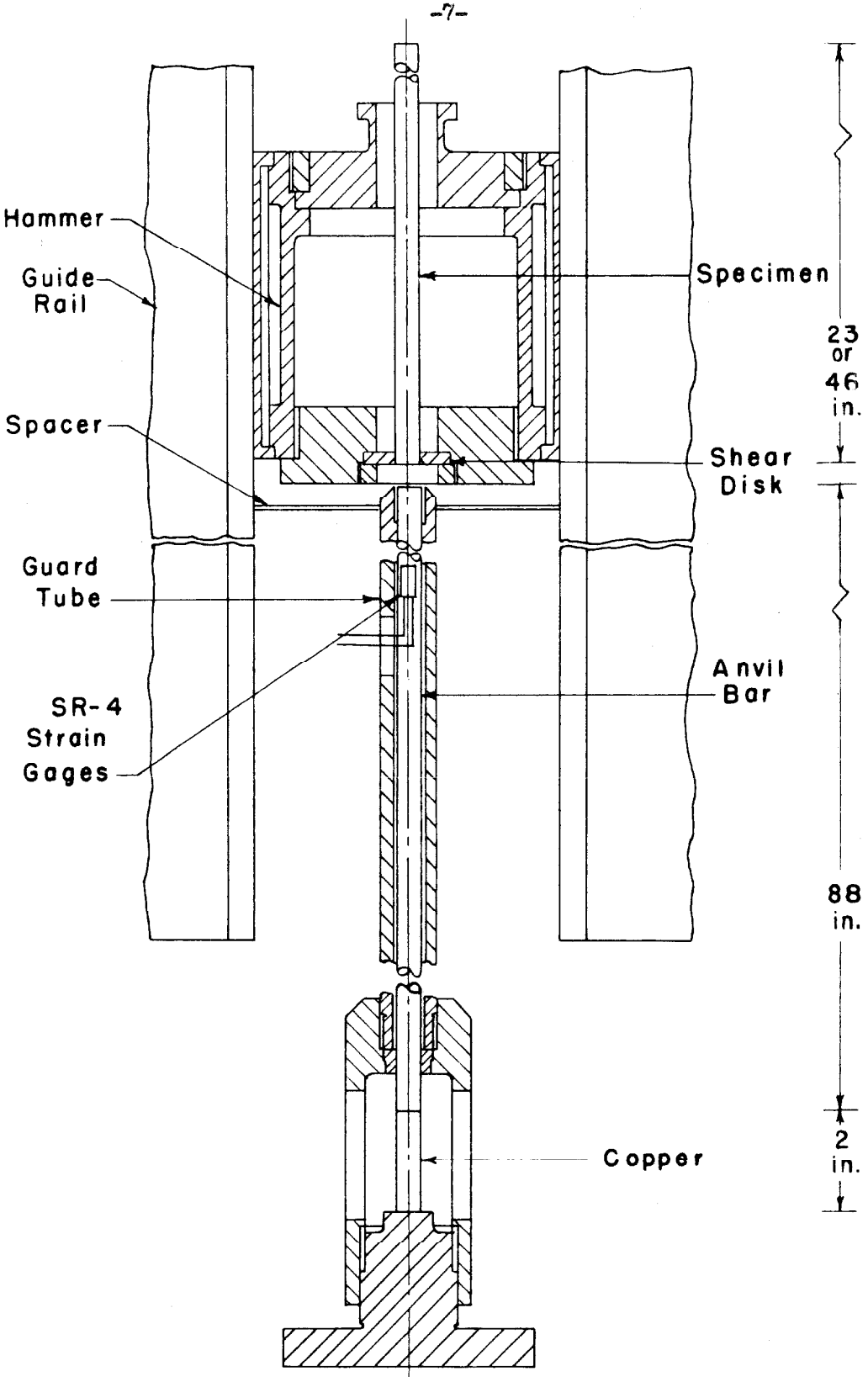

Fig. 2 Section Drawing Vertical Impact Machine

in stress at the interface between the anvil bar and specimen is propagated through the anvil bar at the elastic wave velocity. The length of the specimen is much less than the length of the anvil bar; and hence, the time required for the first reflecting wave from the lower end of the anvil bar to reach the interface between the anvil bar and specimen is greater than the time required for complete unloading of the interface by the waves in the specimen. Thus, the interface between the anvil bar and specimen is always unloaded by waves reflected from the free end of the specimen; and, consequently, all complex reflections from the lower end of the anvil bar need not be considered.

The hammer, which slides on the two vertical rails is provided with a central hole through which the guard tube passes. Twenty rubber bands 3/8 in. thick, 1 in. wide attached to the hammer and frame of the machine serve as a means for accelerating the hammer to the desired impact velocity. The hammer is raised by a lifting mechanism to a height at which the extension of the rubber bands will give the desired velocity. The specimen is held centrally in the hammer by means of a lucite shear disk shrunk onto the bar and clamped in the hammer. The shear disk strikes the top of the guard tube just prior to the impact of the specimen on the anvil bar in such a manner that the specimen is released from the shear disk and

impacts the anvil bar without disturbance from the shear disk. The shear disk fails along the circumference of the clearance hole in the hammer. This allows the hammer to continue downward, passing around the guard tube. It is decelerated by means of four vertical friction brakes. An additional means of decelerating the hammer from high impact velocities is provided by placing a hollow lead cylinder a few feet below the top of the guard tube. The excess kinetic energy of the hammer is converted into kinetic energy and plastic deformation of the lead mass.

Impact velocities less than 19 ft/sec cannot be accurately determined in the vertical impact machine. For this reason, impact velocities lower than 19 ft/sec were obtained by a different method. The specimen is supported in a horizontal position as a pendulum by means of six wires attached at two positions along the specimen. The anvil bar is rigidly supported in a horizontal position such that the specimen when released from a given height centrally impacts the anvil bar at the minimum point in the swing of the specimen. The velocity of impact is determined by measuring the elevation of the specimen prior to release for impact. The velocity of impact could be determined to within $\pm$ 1 per cent.

Recording System:

The velocity of the hammer is determined by measuring

the time to travel between three fixed points near the position of impact. As the hammer passes each of the three fixed points, it closes an electric circuit, causing a discontinuity in the sweep on a cathode-ray oscilloscope screen. A timing trace from an audio oscillator is also placed on the screen of the oscilloscope. The oscilloscope screen is photographed and the number of cycles between the discontinuities is counted, thus giving the time required for the hammer to travel the known distance between the contact points. The accuracy of measurement of the hammer velocity by this method is $\pm$ 2 per cent.

The stress as a function of time at the interface between the anvil bar and specimen is measured during impact by means of SR-4 resistance-sensitive wire gages. Four type AB-14 bakelite bonded gages are cemented to the cylindrical surface of the anvil bar, with their filaments parallel to the longitudinal axis of the anvil bar. The four gages are connected in series, giving a total resistance of 2000 ohms. The strain gages are connected in a voltage dividing circuit which is energized by batteries. Means for introducing known resistance changes are provided in the circuit for calibration of the records. The stress is recorded by a suitable cathode-ray oscilloscope employing a single sweep linear time base.

The anvil bar strain gages were calibrated by placing the anvil bar in a static testing machine. The results of a previous investigation (13) have shown that the sensitivity of the strain gages under impact loads is the same as the sensitivity under static loads. It was found that the stresses determined by the strain gages were within ± 1.2 per cent of the stresses calculated from the impact velocities during an elastic impact.

The response of the recording system was determined by impressing a 5000 cycle/sec square wave having a rise time of less than one-half microsec on the strain gage circuit and recording in the usual manner. The rise time of this square wave on the oscilloscope screen was found to be 30 microsec. This minimum rise time of the recording system imposes a limit on the time which can be accurately resolved on stress-time records.

Plastic Strain Measurements:

The plastic strain in the specimen after impact is determined with a comparator ruling machine. This machine is used for the purpose of marking the specimen at various intervals along its length with a fine scratch before testing and to measure the change in diameter at these positions after impact. The difference between the diameter before and after impact divided by the original diameter is the circumferential

plastic strain. The longitudinal plastic strain is the circumferential plastic strain divided by Poisson's ratio which is assumed to be equal to 0.5 for plastic flow.

The comparator ruling machine consists of a sliding carriage which may be moved over the entire length of a stationary specimen. The position of the carriage is determined by means of a lead screw and a dial graduated in 0.001 in. divisions. A scratching device, a low-power microscope, and a diameter comparator are mounted on the carriage. The scratching device consists of a simple mechanism on which a rigid knife blade is mounted. The low-power microscope is equipped with an eyepiece containing cross hairs which permit the accurate positioning of the carriage at any point along the specimen. The diameter comparator consists of two knife edges in conjunction with a dial indicator for measuring the diameter of the specimen. The specimens are mounted in a position over the carriage on a suitable support parallel to the direction of motion of the carriage.

The combined error in measuring the diameter of the specimen is $\pm$ 0.00006 in. for any given position along the specimen.

TEST PROCEDURE AND EXPERIMENTAL RESULTS

Preparation of Impact Test Specimens:

The specimens used in this investigation were one-half in. diameter extruded 2S aluminum bars. The test specimens were cut from the extruded bars and machined to a length of 23 or 46 in. After machining, the specimens were annealed in a special furnace at 670°F for two hours and furnace cooled to room temperature. The temperature gradient along the specimen length was less than 12°F.

Static Compression and Tension Tests:

Static compression and tension tests were performed in a 150,000 lb Olsen Universal Testing Machine having a least reading of 1 lb (corresponding to a stress of approximately 19 lb/in.^{2} in the gage section of the test specimen). The machine was recently calibrated and showed an error of less than 0.75 per cent. The static compression specimens shown in Fig. 3 were machined from the impact specimens and annealed in the same manner as the impact specimens. Eccentric loading was reduced by placing spherical bearing blocks at each end of the compression test specimen.

Three tests were performed in which the plastic longitudinal and circumferential strain were measured. A given

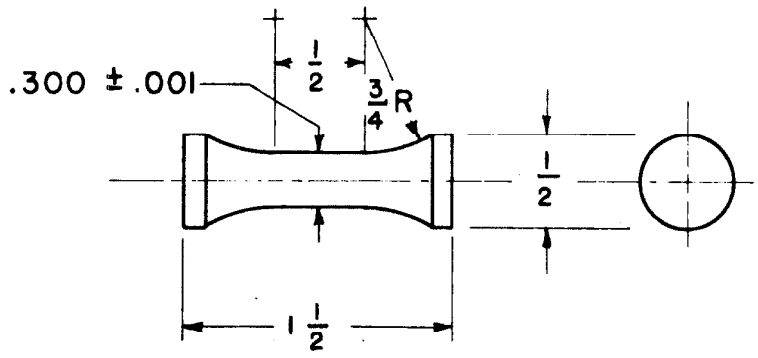

COMPRESSION

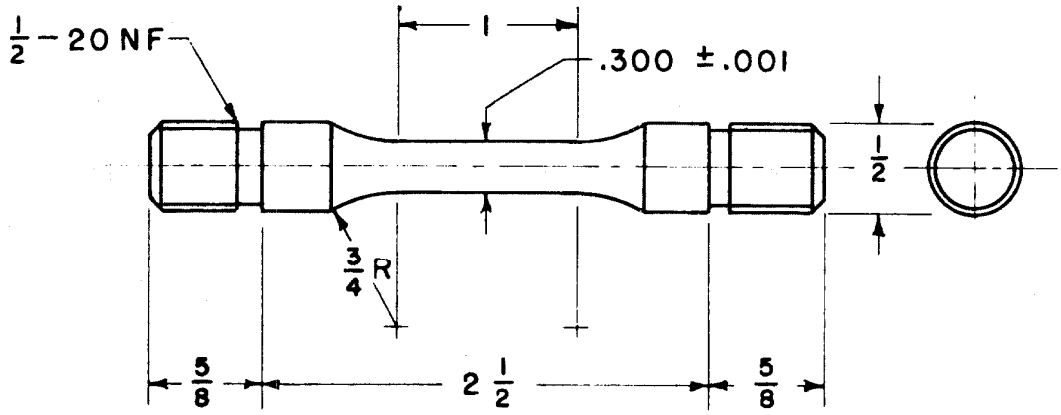

TENSION

Fig. 3 Static Test Specimens

load was applied to the test specimen and maintained for a period of 20 min or until equilibrium was reached. The load was then removed and the plastic strain in the specimen was measured. The longitudinal strain was determined by measuring the change in the distance between pairs of scratched lines on two opposite sides of the test specimen. This change in distance was determined by means of a filar eyepiece and a low-power microscope. The circumferential strain was determined by measuring the change in diameter of the test specimen. The change in diameter divided by the original diameter is the circumferential plastic strain. The longitudinal plastic strain is the circumferential strain divided by Poisson's ratio which is assumed to be equal to 0.5 for plastic flow. The longitudinal plastic strain could be determined to within 0.0004 in./in. by both methods. A comparison was made between the stress-strain relations obtained by the two methods. The comparison indicates that the stress-strain relations obtained by each method are the same within the accuracy of measurement. The mean stress-strain curve up to 10 per cent strain, corrected for elastic recovery upon removal of the load is shown in Fig. 4.

Two continuous loading static compression tests were performed using SR-4 resistance sensitive wire gages to measure the circumferential strain. The circumferential strain

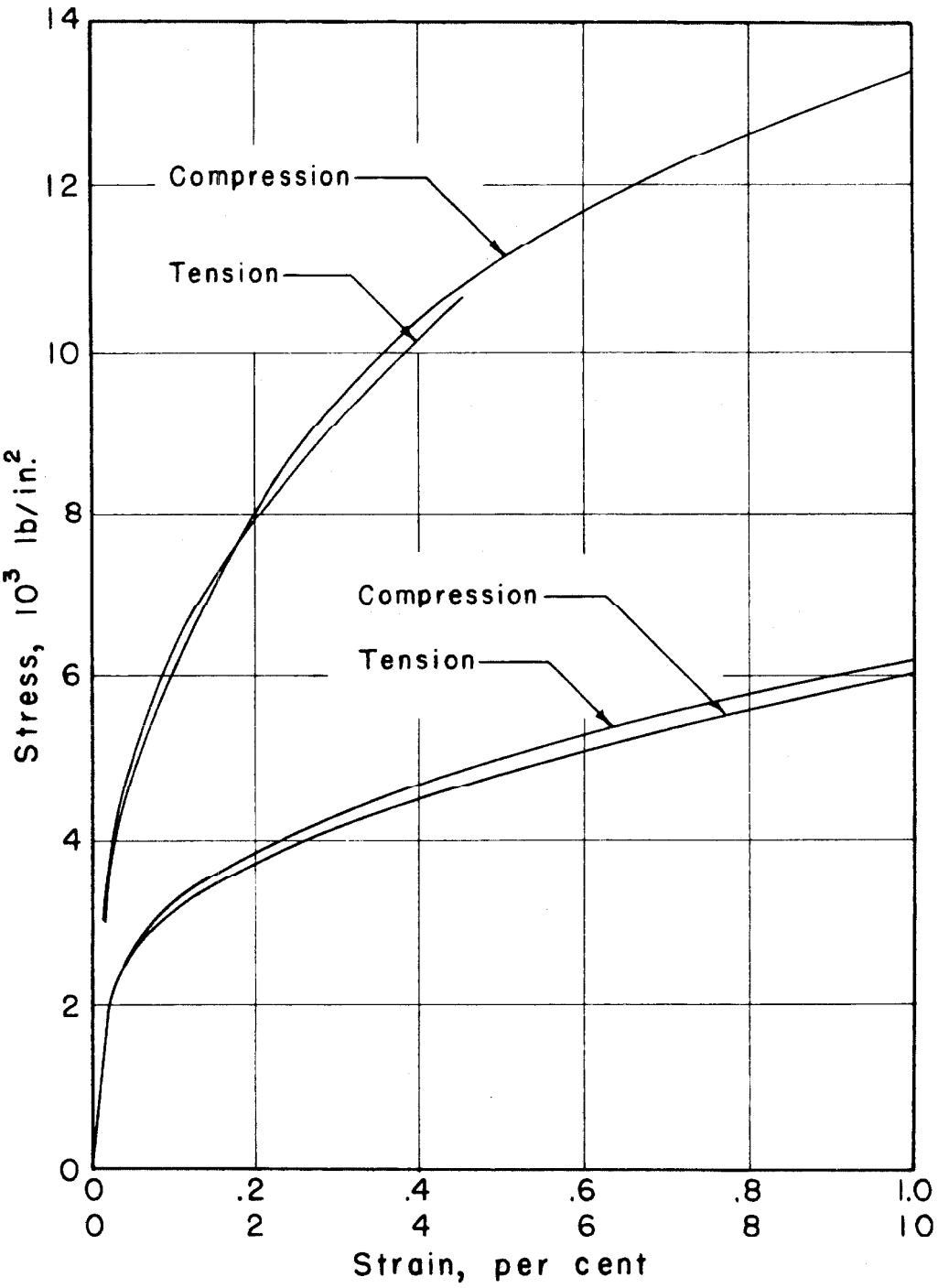

Fig. 4 Static Stress-Strain Relations

could be determined to within ± 2.3 per cent. The longitudinal strain is determined from the equation

$$\varepsilon_L = \frac{-\varepsilon_c}{\nu_p} + \frac{\sigma}{E}\left[1 - \frac{\nu_e}{\nu_p}\right] \qquad (1)$$

where

ε_L is the longitudinal strain,

ε_c is the circumferential strain,

ν_p is Poisson's ratio for plastic flow,

ν_e is theelastic Poisson's ratio,

σ is the compressive stress,

and E is Young's modulus.

The mean static stress-strain curve for the two tests up to 1 per cent strain is shown in Fig. 4.

Four static tension tests were performed to accurately determine the stress-strain relation at low strain values. The static tension specimen is shown in Fig. 3. The strain in the tension specimen was determined with the use of SR-4 resistance-sensitive wire gages and a Holz extensometer having a least reading of 0.000025 in./in. The mean stress-strain curve for the static tension tests is shown in Fig. 4.

A comparison of the static stress-strain relations

obtained by the above methods indicate that for the purpose of this investigation, the longitudinal strain can be accurately determined from circumferential strain measurements.

Determination of the Velocities of Elastic Waves:

The velocities of elastic waves in the specimen and in the tobin bronze anvil bar were determined in order to compute the relations between the strain waves in the specimen and the anvil bar. The elastic wave velocities were determined by measuring the resonance frequency of the bars in longitudinal vibration. The specimen or anvil bar is rigidly clamped at its quarter points which are the nodes for the second mode of vibration. A permanent magnet loudspeaker is placed at each end of the bar with the moving coil cemented to the end of the bar. One of the loudspeakers is driven by an audio oscillator while the other loudspeaker is used as a pickup whose output is displayed on an oscilloscope screen. The resonance frequency of the bar in longitudinal vibration corresponds to the maximum amplitude of the detector signal on the oscilloscope screen.

The velocity of propagation of the elastic wave, c_o, is

$$c_o = \frac{2fl}{n} \qquad (2)$$

where

f is the resonance frequency of longitudinal vibration,

l is the length of the test bar,

and n is the mode of longitudinal vibration.

Young's modulus, E, is also computed from

$$E = \rho c_o^2 \tag{3}$$

where ρ is the mass density of the material.

The results of the determination of the velocities of propagation of elastic waves for the materials used in this investigation are given in Table I. The resonance frequencies are given for the second and third modes of vibration. The latter could be obtained since the nodal points for the third mode are very near the quarter points of the bar. The elastic wave velocities are computed for each test, and the average velocity in each material is also given. Young's modulus of each material is computed from the average elastic wave velocity and the mass density, ρ. The value of ρ given for each material in Table I is an average of three densities obtained by weighing a known volume of the material. It is estimated that the accuracy in the determination of elastic wave velocities is within $\pm$ 0.6 per cent. The deviation of values of elastic wave velocities from the mean value is less than 0.7 per cent.

TABLE I

ELASTIC WAVE VELOCITIES AND MODULI OF ELASTICITY

Test Number	Length in.	Mode	Resonance Frequency Cycles/sec	Elastic Wave Velocity in./sec	Modulus of Elasticity 10^6 lb/in.^{2}
	Determinations on Annealed 2S Aluminum				
	$\rho = 2.54 \times 10^{-4}$ lb sec^2/in.^{4}				
1	48	2	4076	195,600	
2	48	2	4062	195,000	
3	48	3	6154	196,900	
4	48	2	4084	196,000	
5	47 31/32	2	4065	195,000	
6	47 31/32	2	4060	194,800	
7	47 31/32	2	4060	194,800	
8	47 31/32	3	6110	195,400	
			Average	195,400	9.71
	Determinations on Anvil Bar (tobin bronze)				
	$\rho = 7.85 \times 10^{-4}$ lb sec^2/in.^{4}				
9	87 13/16	2	1587	139,200	
10	87 13/16	2	1589	139,600	
11	87 13/16	3	2387	139,700	
12	87 13/16	3	2391	139,900	
13	87 13/16	2	1585	139,100	
			Average	139,500	15.2

Compression Impact Tests:

A series of tests was made to determine the relations between the maximum compression stress at the impact end of the specimen, the plastic strain distribution in the specimen after impact, and the velocity of impact. The velocity of impact is defined as the velocity of the specimen just prior to the impact of the specimen on the anvil bar. Since the anvil bar is elastic, the change in velocity of the impacted end of the specimen upon impact is not equal to the velocity of impact. The change of velocity upon impact is defined as the particle velocity, v. This is equivalent to assuming that the end of a stationary specimen is suddenly put into motion with a constant velocity, v.

The particle velocity at the impact end of the specimen is determined by satisfying the continuity of stress and particle velocity at the interface of the test specimen and the anvil bar. The particle velocity, v, is given by

$$v = V_o - \frac{\sigma_m}{\bar{\rho} c_o} \qquad (4)$$

where

V_o is the velocity if impact,

σ_m is the maximum compression stress at the interface,

$\bar{\rho}$ is the mass density of the anvil bar,

and c_o is the velocity of propagation of an elastic wave

in the anvil bar. Impact velocities were chosen to obtain a uniform distribution of test points in the plot of σ vs. v. A tracing of a record of stress vs. time at the impact end of the specimen is shown in Fig. 5.

The results of the compression impact tests are summarized in Table II. The plastic strain distribution in the specimen after impact was determined for most of the tests. The maximum plastic strain near the impact end of the specimen for these tests is also given in Table II. Impact velocities from 19.2 to 125 ft/sec were obtained in the vertical impact machine. Impact velocities from 3.15 to 15.9 ft/sec were obtained by supporting the specimen horizontally as a pendulum. The points representing the particle velocity as a function of maximum compression stress at the impact end of the specimen are plotted in Fig. 6. The points representing maximum compression stress as a function of the measured strain near the impact end of the specimen are plotted in Fig. 7. The strains are corrected for the elastic recovery upon removal of the load.

The experimentally determined relationship of particle velocity vs. compression stress shown in Fig. 6 is the relation between the maximum compression stress and particle velocity at the impact end of the specimen. The stress-strain curve during impact conditions can be deduced from this relation if

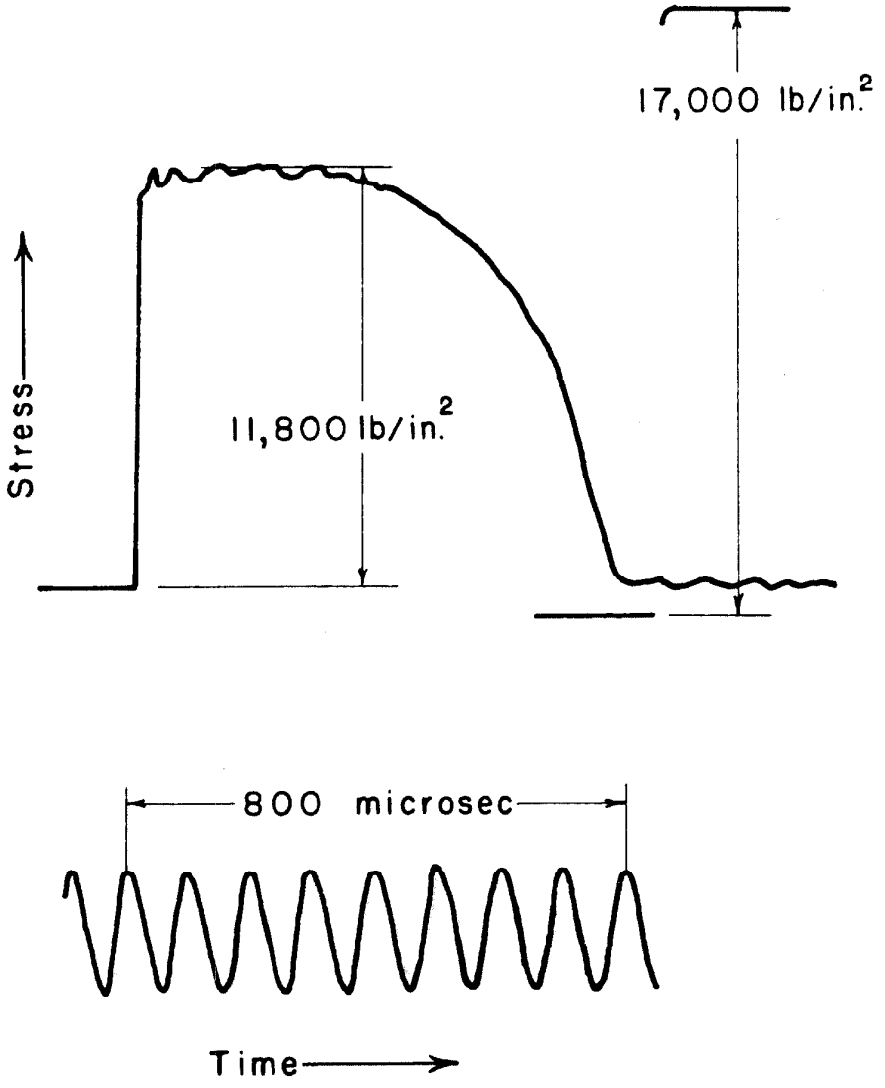

Fig. 5 Tracing of a Record of Stress vs. Time, Impact Velocity 98.5 ft/sec, Specimen No. 18A

TABLE II

RESULTS OF COMPRESSION IMPACT TESTS

Specimen Number	Maximum Stress $10^3 lb/in^2$	Velocity of Impact ft/sec	Maximum Particle Velocity ft/sec	Maximum Permanent Strain per cent
20A	1.30	3.15	2.16	-
21C	1.82	4.50	3.12	-
20B	2.43	6.21	4.36	-
20C	2.78	8.00	5.88	-
20D	2.90	9.82	7.61	-
21B	3.23	10.0	7.54	-
40A	3.35	12.4	9.83	-
40B	3.84	14.6	11.6	-
6A	4.12	16.8	13.6	0.30
5A	4.17	16.8	13.6	0.35
21A	4.21	15.9	12.7	-
19F	4.65	19.2	15.7	0.25
5F	5.07	19.7	15.8	0.35
22C	5.23	25.3	21.3	0.45
5E	5.74	26.6	22.2	0.50
22D	5.81	29.9	25.5	0.55
19E	5.87	31.1	26.6	0.70
23A	6.23	33.2	28.5	0.70
19D	6.36	37.6	32.8	0.90
23B	6.68	38.2	33.1	0.90
4E	7.45	43.9	38.2	1.10
4D	7.52	45.8	40.1	1.10
4C	7.56	44.8	39.0	1.10
4B	7.58	44.3	38.5	1.10
4F	7.60	45.4	39.6	1.05
4A	7.65	44.9	39.1	1.10
1A	7.68	44.5	38.6	1.20
1B	8.22	52.0	45.7	1.45
1C	8.82	58.2	51.5	1.65
1D	9.39	67.1	60.0	1.90
5D	9.48	71.6	64.4	2.05
1E	9.94	70.8	63.3	2.20
1F	9.98	76.0	68.4	2.35

TABLE II continued

Specimen Number	Maximum Stress 10^3 lb/in.^{2}	Velocity of Impact ft/sec	Maximum Particle Velocity ft/sec	Maximum Permanent Strain per cent
35A	10.4	80.0	72.1	2.65
35B	10.6	87.5	79.4	2.85
17E	11.5	97.0	88.3	3.20
18A	11.8	98.5	89.5	3.40
18B	12.2	103	93.9	3.65
19A	12.4	122	113	3.85
18C	12.5	111	102	4.00
18D	12.8	115	106	4.15
18E	13.0	123	113	4.65
18F	13.4	125	115	4.80

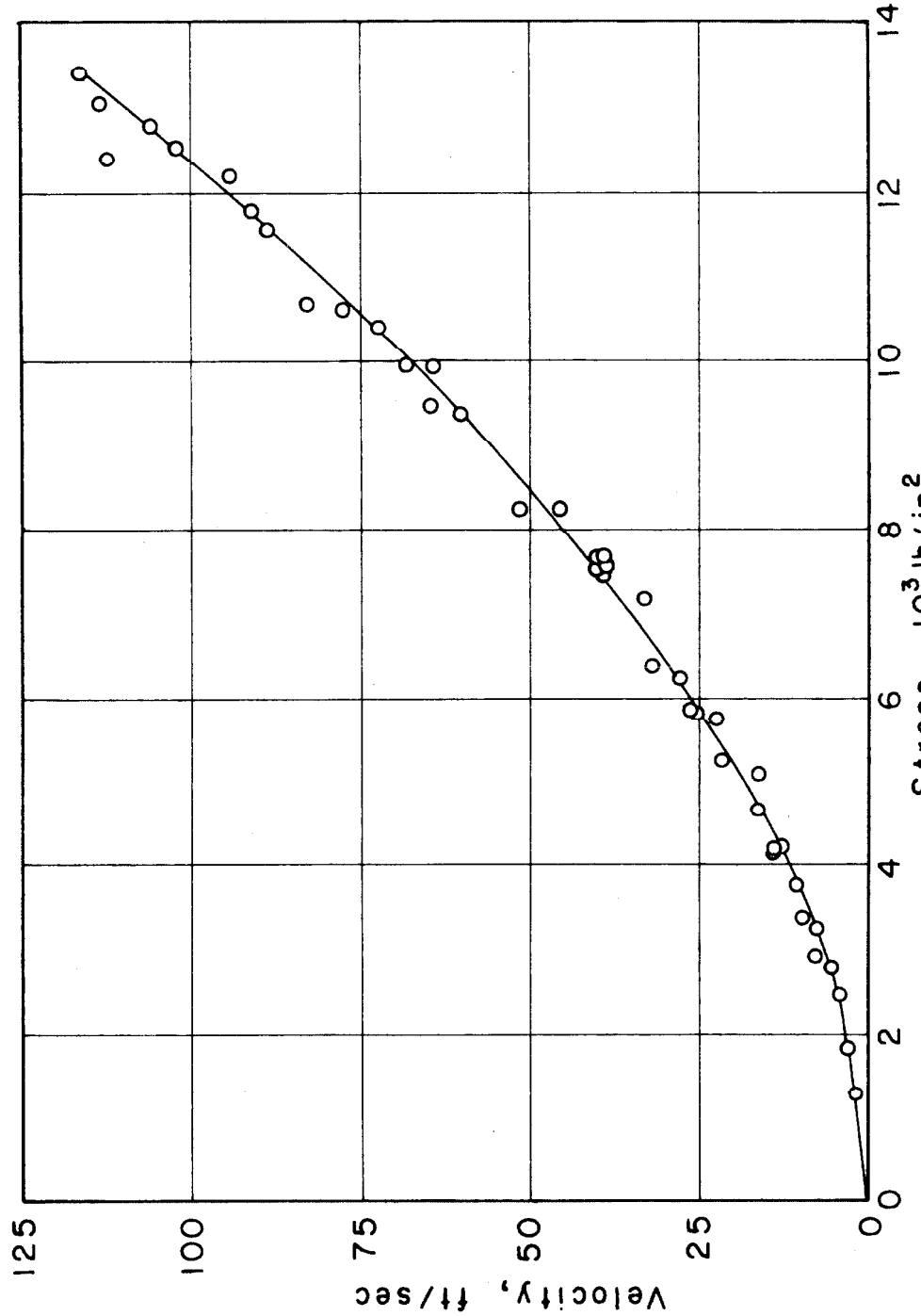

Fig. 6 Impact Stress vs. Particle Velocity

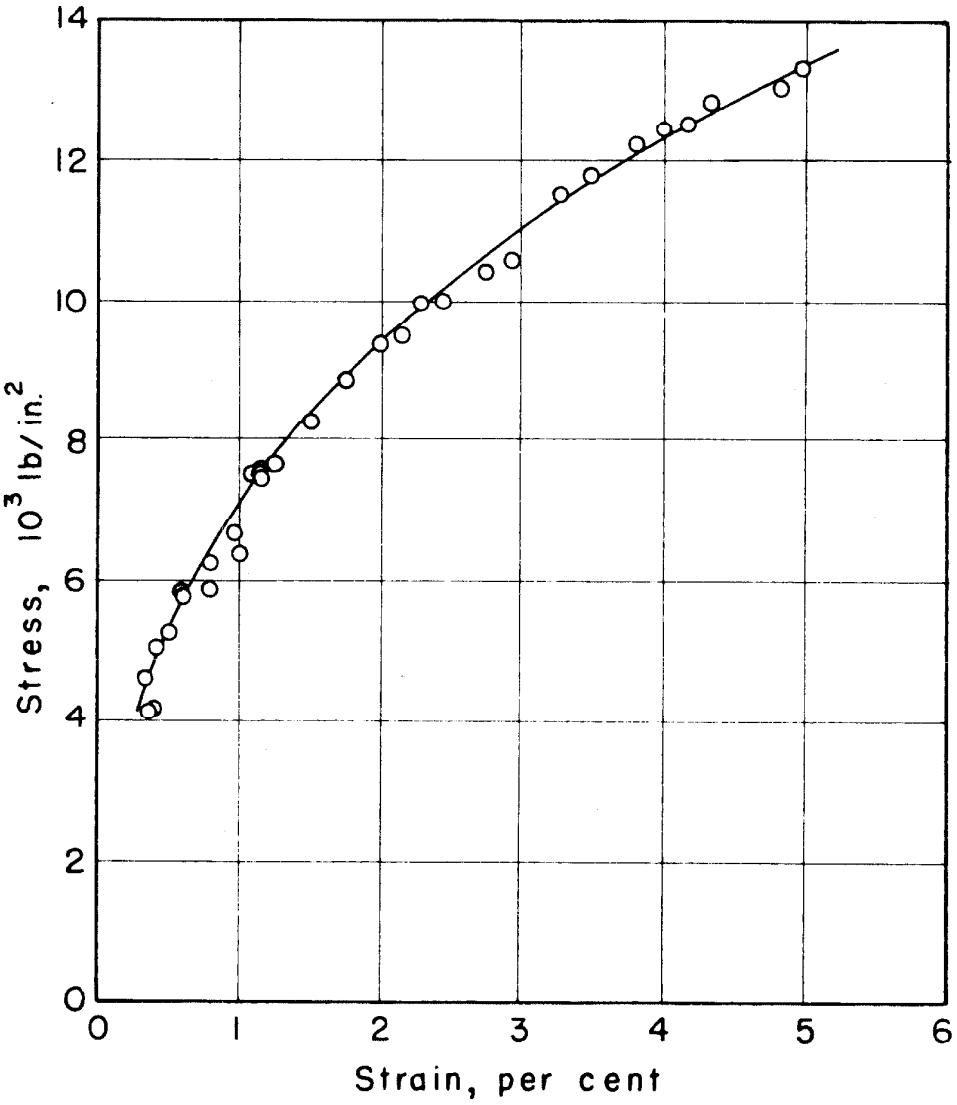

Fig. 7 Impact Stress vs. Maximum Plastic Strain

the following assumption are made. First, it is assumed that the stress-particle velocity relationship during loading follows this curve continuously up to the point corresponding to the given impact velocity. It is possible however, that this relation may represent the locus of the terminal points of a number of distinct stress-particle velocity curves which depend upon the given impact velocity. Second, it is assumed that the kinetic energy and shear stresses associated with the lateral motion of the particles of the specimen can be neglected. The theoretical relation obtained under these assumptions will later be compared with other experimental results to determine the validity of these assumptions.

These assumptions permit the use of the theory of longitudinal waves of plastic deformation in long thin bars developed by von Karman (15-16). The strain for a given stress can be expressed in terms of a definite integral which depends upon the slope of the stress-particle velocity curve up to the given stress. A certain velocity of propagation is associated with each value of plastic strain as given by the following form

$$c = \sqrt{\frac{d\sigma}{d\varepsilon}/\rho} \qquad (5)$$

where

c is the velocity of propagation,

ρ is the mass density of the material,

σ is the stress,

and ε is the strain. The velocity of propagation for a given strain is also equal to the slope of the v vs. ε curve at this strain. This is given by

$$c = \frac{dv}{d\varepsilon} . \tag{6}$$

The slope of the stress-strain curve, $\frac{d\sigma}{d\varepsilon}$, is determined from equations (5) and (6). It is expressed by the following equation

$$\frac{d\sigma}{d\varepsilon} = \left(\frac{d\sigma}{dv}\right)^2 \Big/ \rho \quad .$$

The strain, ε_1, corresponding to a given stress, σ_1, on the σ vs. v curve shown in Fig. 6 is computed from the equation

$$\varepsilon_1 = \int_0^1 \frac{\rho \, d\sigma}{\left(\frac{d\sigma}{dv}\right)^2} . \tag{7}$$

The slope of the σ vs. v curve shown in Fig. 6 is determined at conveniently located points and the quantity given by equation (7) is plotted for each of the corresponding stresses, σ_1. This stress-strain relation is shown in Fig. 8 by the curve designated as stress-velocity measurements. The static stress-strain curve and stress-strain relation determined from maximum compression stress-measured plastic strain are shown for comparison. The latter is designated by the curve, stress-plastic strain measurements.

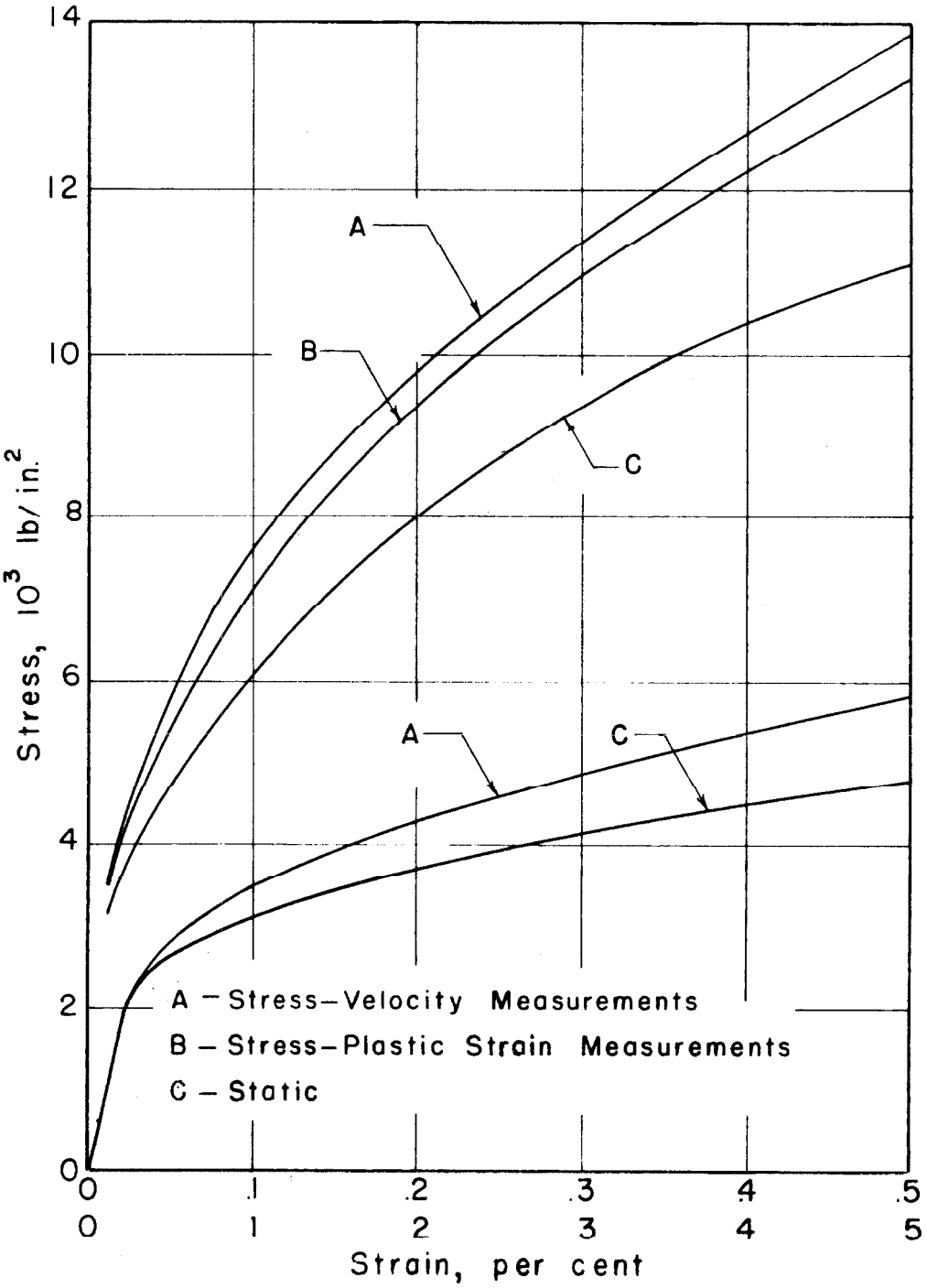

Fig. 8 Dynamic Stress-Strain Relations

The stress-strain curve deduced from maximum stress-velocity measurements is somewhat different from the curve determined from maximum stress-measured strain. Thus, for a given stress, the strain deduced from stress-velocity measurements with the use of the theory of plastic wave propagation is less than the measured strain after impact. However, the stress-strain relation given by either of these curves lies considerably above the static stress-strain curve. Therefore, under impact conditions, the stress for a given strain is greater than the stress under static conditions. A further investigation was made to determine if this increase in stress of the material is associated with the extremely high loading rates in impact or if the increase could be obtained by moderate loading rates.

Moderate Loading Rate Tests:

The moderate loading rate tests were performed in a rapid load testing machine by manipulating the load actuating mechanism in such a manner that a nearly constant rate of strain was obtained. The specimens were the same as the static tension specimens shown in Fig. 3. The load acting on the specimen was measured by means of a dynamometer employing type AB-14, SR-4 strain gages with suitable temperature compensation. The strain in the specimen was measured by means

of an extensometer employing similar SR-4 strain gages. The load and the strain were recorded on photographic paper by a recording oscillograph. Timing lines at intervals of 0.1 sec were projected onto the test record to provide a time base. The stress could be determined to within ± 1.5 per cent and the strain to within ± 1 per cent. Two loading rates were used. These loading rates corresponded to strain rates of 0.011/min and 0.040/min. The stress-strain curves for the two rates are shown in Fig. 9 with the static stress-strain curve.

The results indicate that the relatively large increase in stress over the static value for a given strain is associated with the extremely ~~fast~~ high loading rates in impact. Thus, the stress-strain relation for the material used in this investigation obtained under impact conditions is not the same as the stress-strain relation under static or moderate loading rates. It is evident that a dynamic stress-strain curve must be used to describe the process of propagation of plastic deformation. The plastic strain measured after impact may not represent the value of strain associated with the propagation process. The measured plastic strain may be the sum of plastic strain due to initial impact and an additional strain due to relaxation of the material. Since the stress at the impact end of the specimen and the impact velocity were

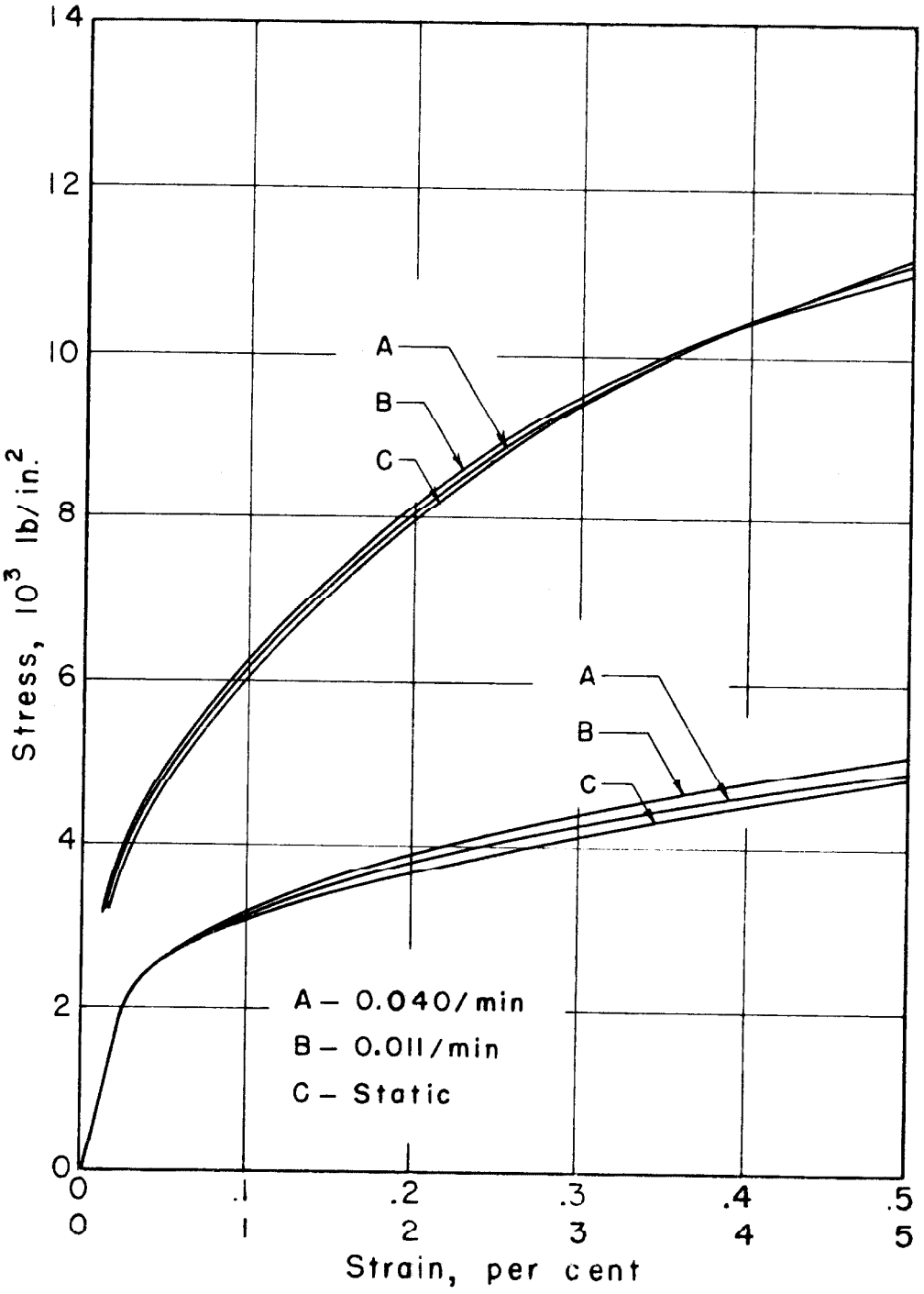

Fig. 9 Stress-Strain Relations under Moderate Loading Rates

measured during impact, the relation determined from these measurements may be more representative of the behavior of the material under impact conditions than the dynamic curve determined from strain measurements after impact.

Lagrange Diagram:

The process of wave propagation in the specimen can be deduced from a stress-strain relation of the material. The wave propagation process is represented in a Lagrange or position-time diagram from which the stress, strain, and particle velocity are determined as a function of position and time. Thus, the stress-time, strain-time, and strain-position relations deduced from this stress-strain relation can be compared with the experimentally determined relations. The theory and graphical solutions for strain propagation problems were developed by von Karman, Bohnenblust, Myers, and Charyk (17-18). The details of the method of constructing a Lagrange diagram from a stress-strain relation are given in the appendix.

The dynamic stress-strain curve deduced from maximum stress-impact velocity measurements shown in Fig. 8 is used in constructing the Lagrange diagram. It is assumed that the stress-strain path during loading follows this stress-

strain relation. The Lagrange diagram shown in Fig. 10 is constructed for the maximum velocity of impact employed in the impact tests. The line, x = 0, represents the interface between the anvil bar and test specimen. The line, x = - 3 in., represents the position of the strain gages on the anvil bar. The heavy irregular line represents the boundary between the plastic and hysteresis regions for the maximum impact velocity while the heavy dashed lines represent similar boundaries for lower impact velocities.

Stress as a function of time at the interface between the tests specimen and anvil bar is determined from the Lagrange diagram. The theoretical stress-time relations for four impact velocities are shown in Figs. 11, 12, 13, and 14. The corresponding experimental relations obtained from stress-time measurements are also shown for comparison.

The theoretical plastic strain distribution is also determined from the Lagrange diagram. Three plots of plastic strain as a function of the distance along the specimen are shown in Figs. 15, 16, and 17. The corresponding experimental plastic strain distributions measured after impact are also shown for comparison.

The plastic strain distributions shown in Figs. 15, 16, and 17 indicate that the maximum plastic strains at the impact end of the specimen which are computed from the

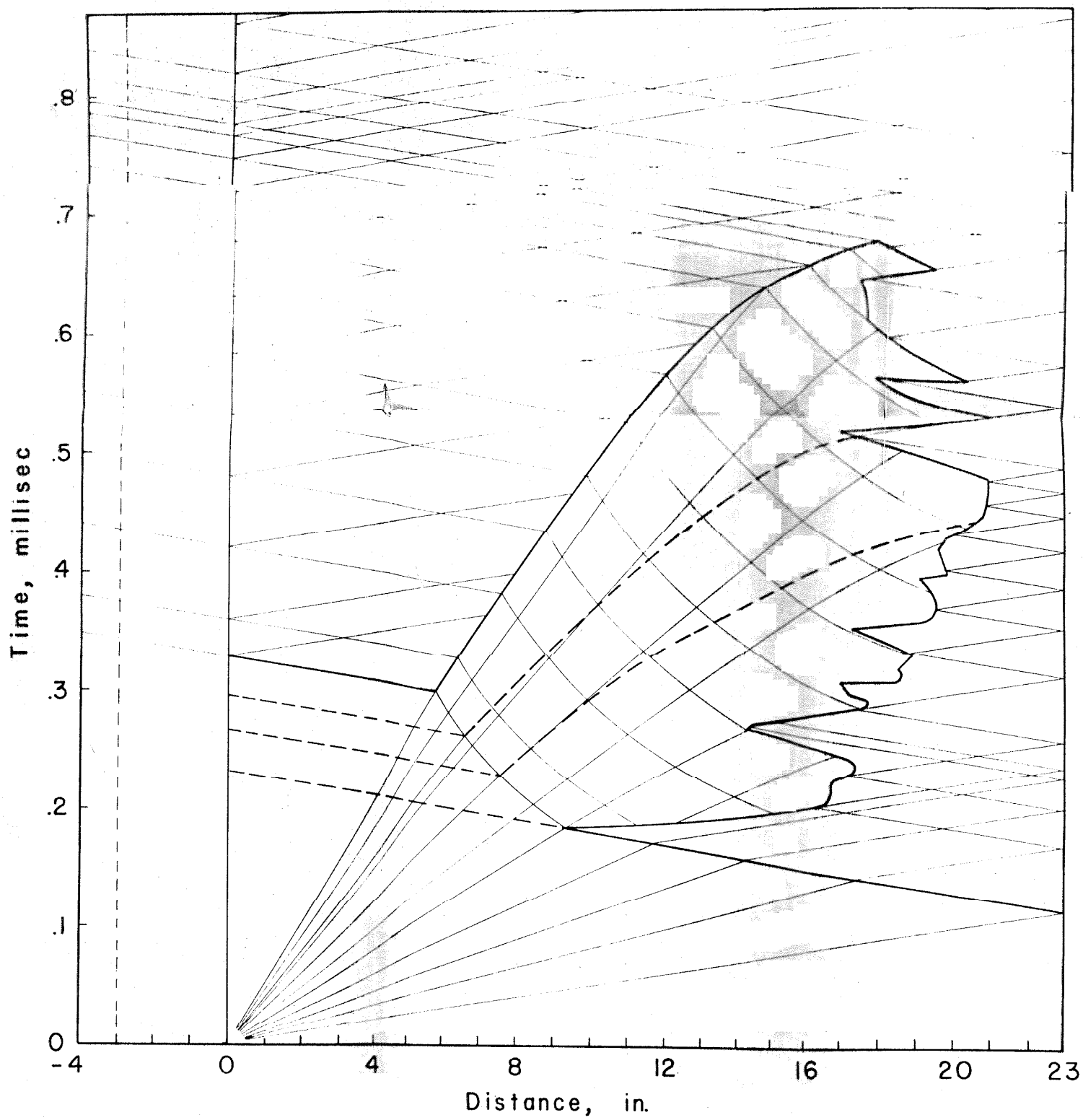
.8
.7
.6
.5
.4
.3
.2
.1
0
Time, millisec
-4
0
4
8
12
16
20
23
Distance, in.

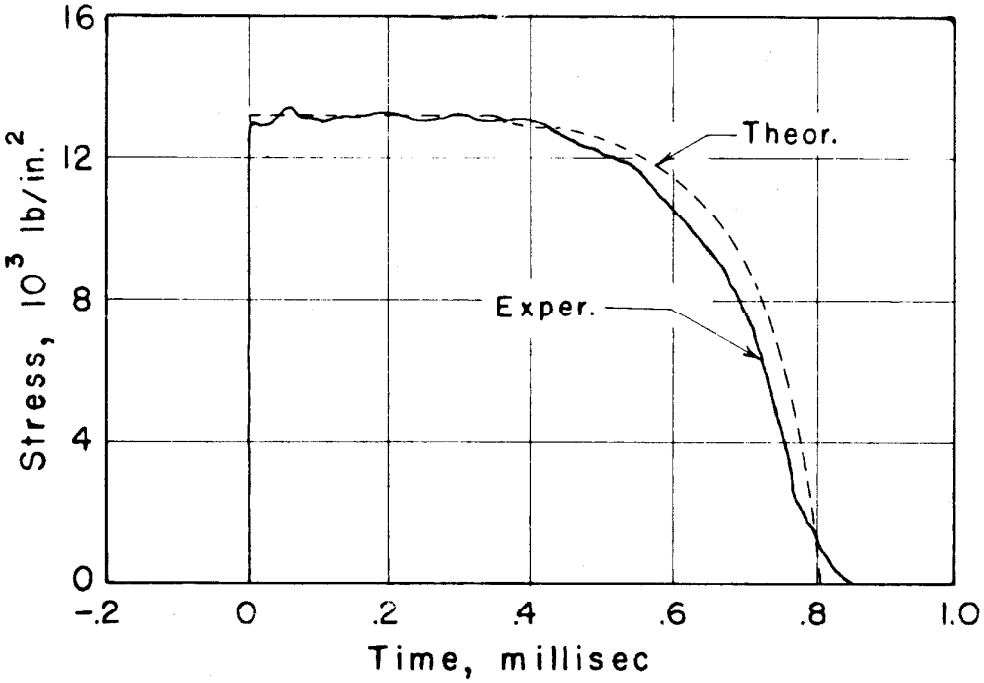

Fig. 11 Stress vs. Time, Impact Velocity 123 ft/sec, Specimen No. 18A

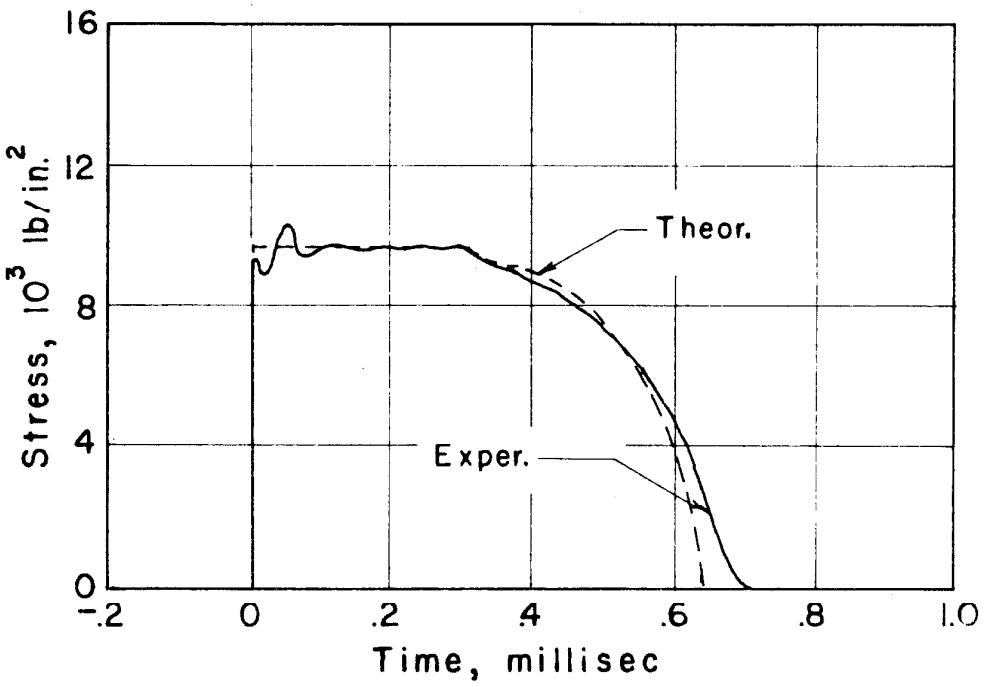

Fig. 12 Stress vs. Time, Impact Velocity 71.6 ft/sec, Specimen No. 5D

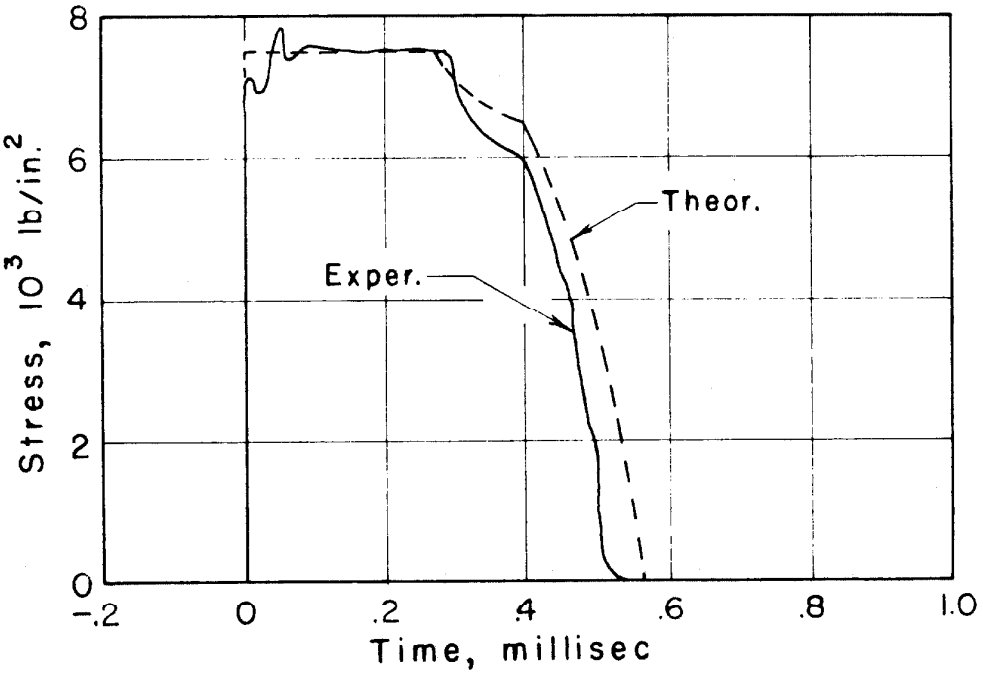

Fig. 13 Stress vs. Time, Impact Velocity 45.8 ft/sec, Specimen No. 4D

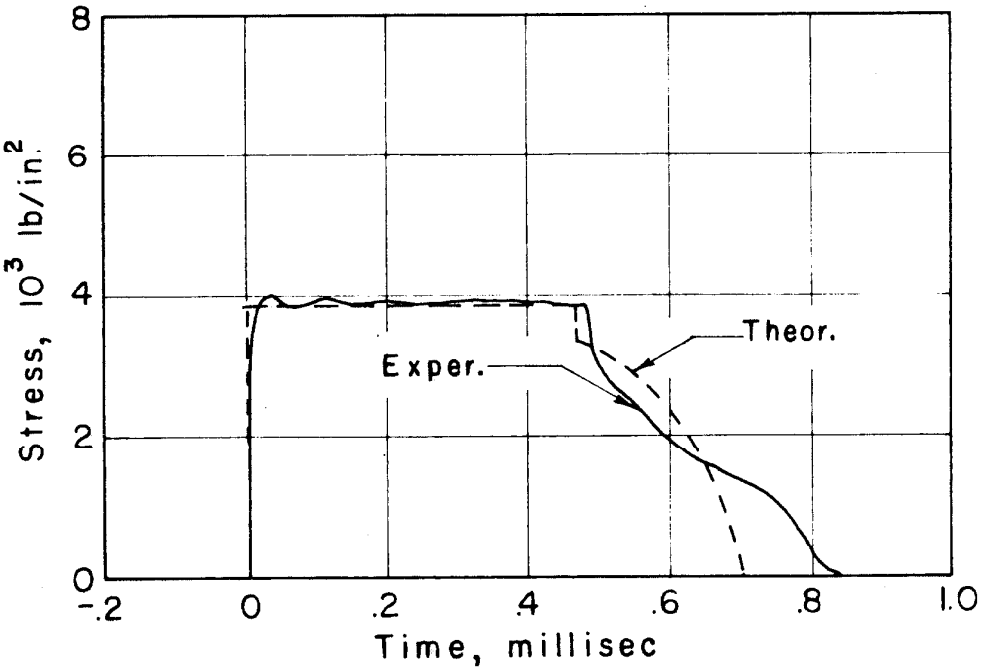

Fig. 14 Stress vs. Time, Impact Velocity 14.6 ft/sec, Specimen No. 40B

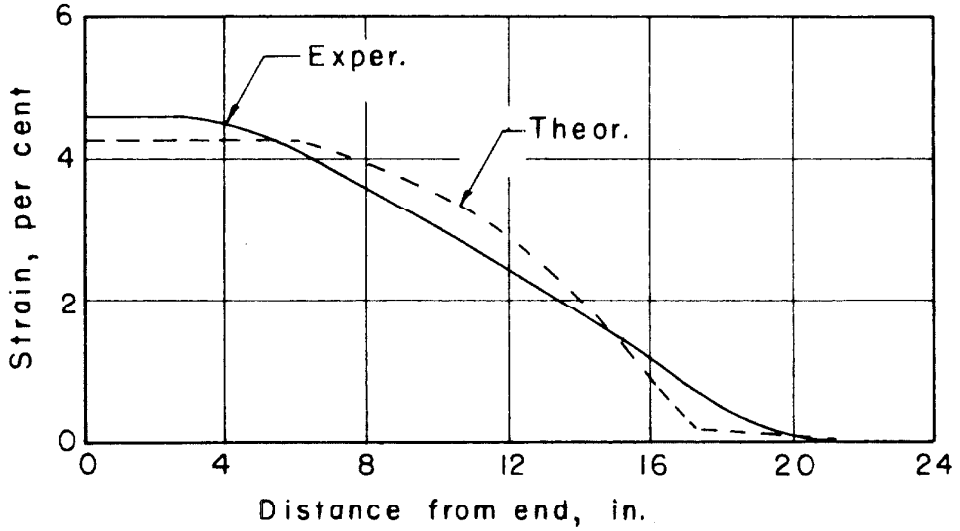

Fig. 15 Plastic Strain Distribution, Impact Velocity 123 ft/sec, Specimen No. 18E

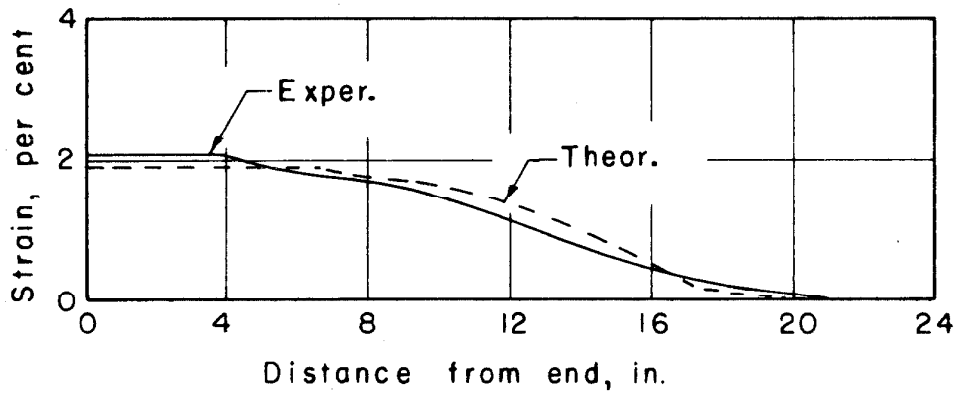

Fig. 16 Plastic Strain Distribution, Impact Velocity 71.6 ft/sec, Specimen No. 5D

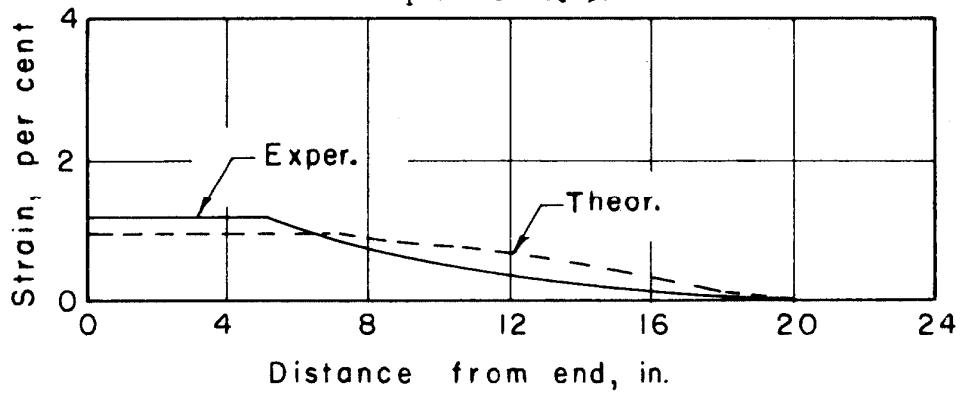

Fig. 17 Plastic Strain Distribution, Impact Velocity 45.8 ft/sec Specimen No. 4D

Lagrange diagram are not equal to the measured strains. The measured plastic strain near the impact end of the specimen is greater than the maximum plastic strain computed from the Lagrange diagram. A comparison of other plastic strain distributions indicates that in nearly every case the measured maximum strain is greater than the computed maximum strain. For this reason, strain as a function of time during impact was determined experimentally at several positions along the bar in an attempt to explain the discrepancy.

The strain in the specimen as a function of time was determined during impact with the use of SR-4 resistance sensitive wire strain gages cemented to the specimen. Gages were mounted in such a manner that the circumferential strain was recorded. In this manner, tension strains are measured. This was considered necessary since the reliability of wire strain gages at large values of compressive strains is uncertain (19). One channel of the recording system was used to determine stress-time at the impact end of the specimen in the usual manner and the other channel was used for strain-time measurements. A reference timing mark was simultaneously impressed on each oscilloscope screen trace of stress-time and strain-time in order to establish the time at impact on the strain-time record.

Four typical experimental strain-time records

are shown in Figs. 18, 19, 20, and 21. The strain-time relations are also determined theoretically from the Lagrange diagram and shown in the figures for comparison. The results indicate that the maximum strain determined from strain-time records near the impact end of the specimen is comparable with the measured strain after impact. Furthermore, this maximum strain is obtained during the initial loading of the specimen and the strain remains nearly constant after this maximum strain is reached.

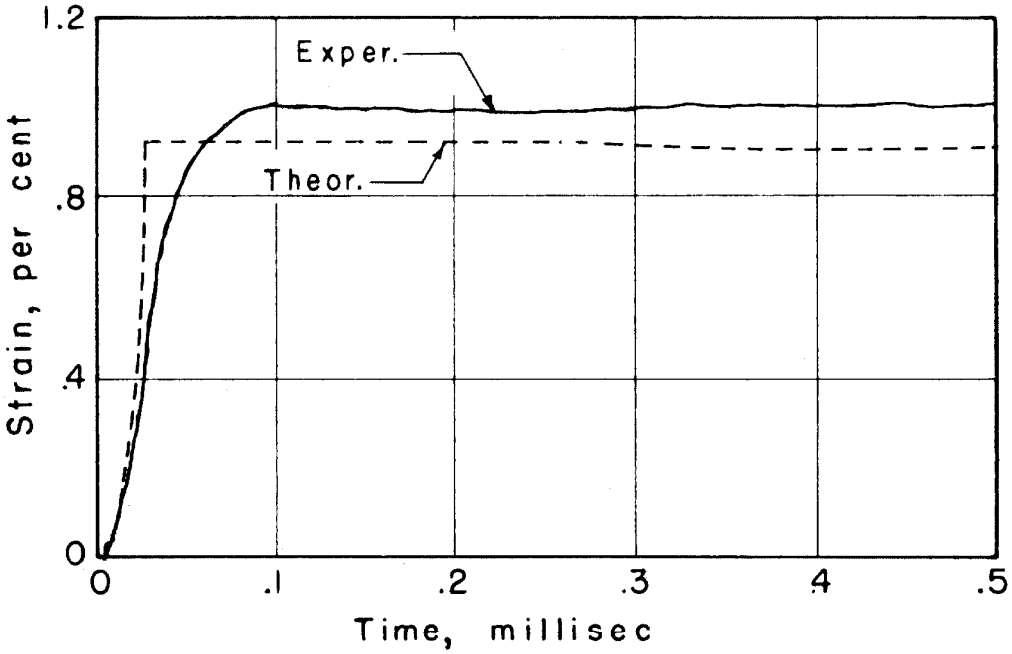

Fig. 18 Strain vs. Time, Impact Velocity 44.7 ft/sec, 0.9 in. from End, Specimen No. 9A

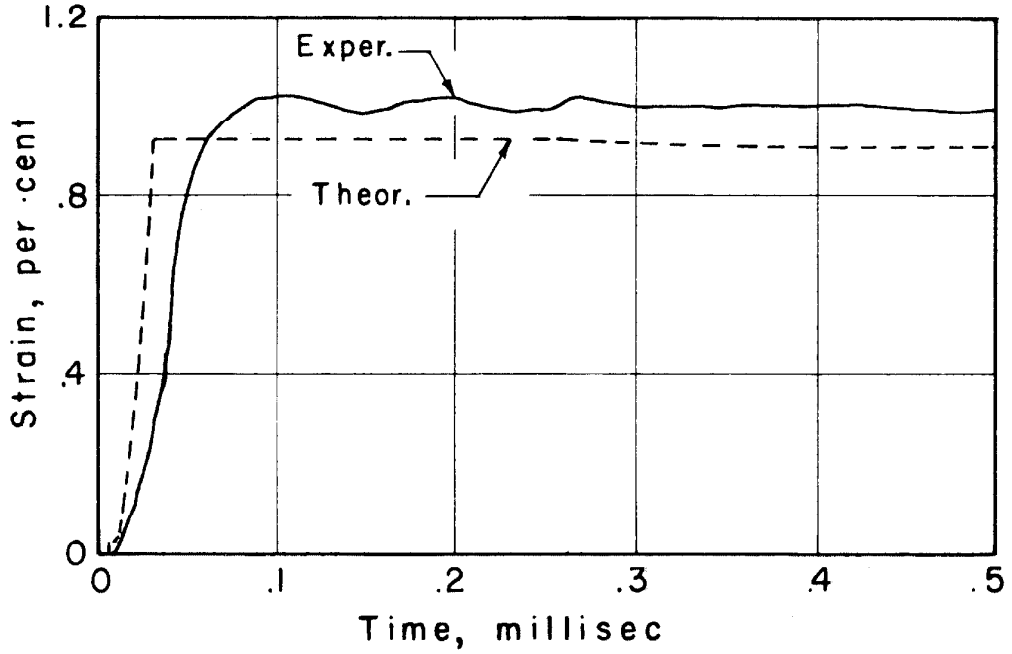

Fig. 19 Strain vs. Time, Impact Velocity 44.7 ft/sec, 1.0 in. from End, Specimen No. 12A

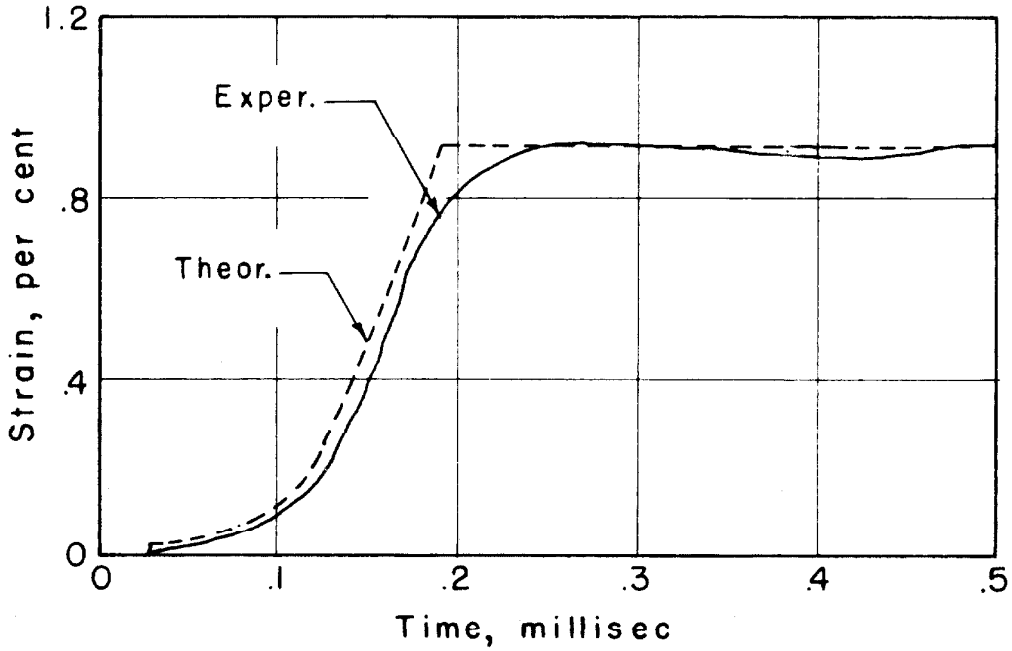

Fig. 20 Strain vs. Time, Impact Velocity 44.7 ft/sec, 6.0 in. from End, Specimen No. 13A

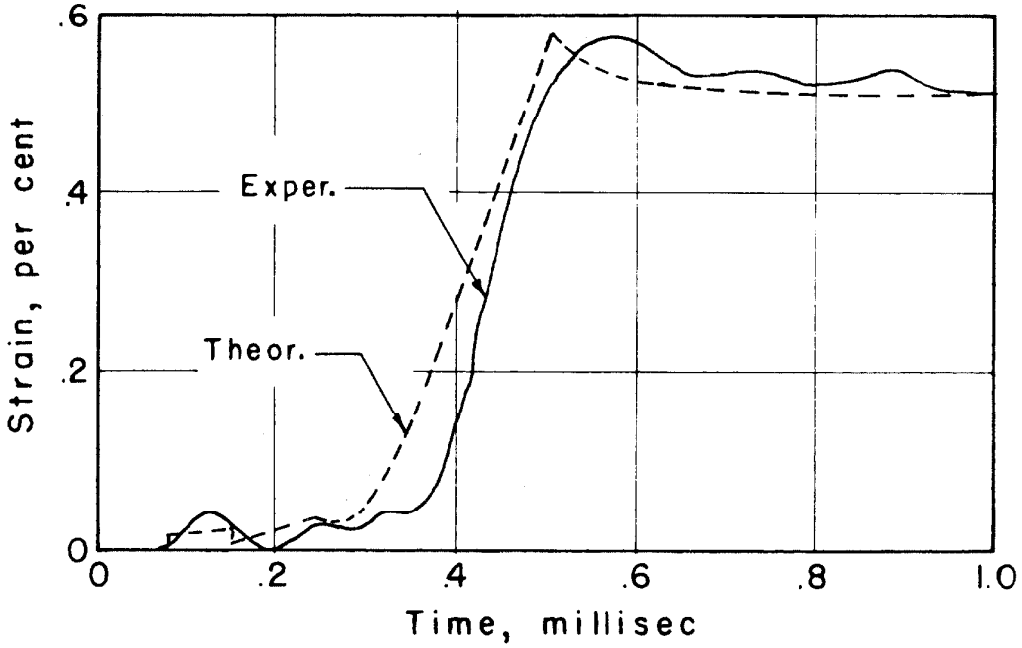

Fig. 21 Strain vs. Time, Impact Velocity 69.8 ft/sec, 16.0 in. from End, Specimen No. 24A

DISCUSSION OF RESULTS

The experimental results indicate that the stress-strain relation deduced from stress-velocity measurements with the use of the theory of propagation of plastic strains lies above the stress-strain relation determined from stress-plastic strain measurements. Thus, for a given stress, the strain deduced from stress-velocity measurements is less than the strain measured after impact. This can be seen in Fig. 8. This discrepancy between the two stress-strain curves cannot be explained by experimental errors or errors due to construction of the curves. A dynamic stress-strain relation determined from either stress-velocity measurements or stress-plastic strain measurements lies considerably above the static stress-strain relation. The dynamic stress-strain curve determined by either of the methods is representative of the behavior of the material when the load duration is of the order of one millisec. Thus, the increase in stress over the static value for a given strain can be considered as a primary effect which accompanies the increased loading rates prevailing under impact conditions. The discrepancy between the two dynamic curves deduced from stress-velocity measurements and stress-plastic strain measurements can be considered as a secondary effect.

If a constant stress is applied to the end of a semi-infinite bar by compression impact, an initial stress and strain are reached at the impact end which correspond to a point on the dynamic stress-strain curve. This position on the dynamic stress-strain curve cannot be maintained indefinitely and the stress and strain must approach some equilibrium position on the static stress-strain curve. In this investigation, the specimen is of finite length, and, consequently, is unloaded by the reflection of waves from the free end. The relaxation of stress and/or strain from the dynamic curve to the static curve is interrupted by the unloading of the specimen. The magnitude of this relaxation can be estimated from the stress-time records at the impact end of the specimen and compared with the difference between the measured and calculated maximum plastic strain. The stress-strain relation during relaxation cannot be determined from the experimental data, but the overall magnitude of the relaxation can be estimated.

When the specimen strikes the stationary anvil bar, an initial stress and strain are reached. The initiation of any additional plastic strain at the interface after the initial impact is accompanied by a compression plastic strain propagating through the specimen. An unloading tension wave traveling at the elastic wave velocity must also be

propagated through the specimen and anvil bar to satisfy the continuity of stress and particle velocity at the interface. Thus, any increase in strain after the initial strain must be accompanied by a decrease in stress at the interface. However, the experimental stress-time records at the interface indicate that during impact the stress at the impact end of the specimen remains nearly constant. This can be seen in Figs. 11, 12, 13, and 14. A decrease in stress due to relaxation cannot be observed if the change of stress is less than the variation of stress along the nearly constant portion of the stress-time record. This variation of stress imposes an upper limit on the stress decrease that can be attributed to relaxation. The magnitude of this decrease in stress, $\Delta \sigma_1$, due to relaxation is determined from the Hugoniot relations of stress and particle velocity and is given by

$$\Delta \sigma_1 = \Delta \sigma_2 \left[\frac{1 - \frac{c_o}{c}}{1 + \gamma} \right] \qquad (8)$$

where $\Delta \sigma_2$ is the incremental stress increase due to the compression wave in the specimen,

c is the compression wave velocity,

c_o is the elastic wave velocity in the specimen,

and γ is the acoustic impedance of the specimen, ρc_o,

divided by the acoustic impedance of the bar, $\overline{\rho c_o}$. The Hugoniot relation of the strain, $\Delta\varepsilon_2$, associated with the incremental stress, $\Delta\sigma_2$, is given by

$$\Delta\sigma_2 = \rho c^2 \Delta\varepsilon_2 . \qquad (9)$$

If a strain increase due to relaxation occurs, the magnitude of this strain can be determined from equations (8) and (9). It is assumed first that the compression wave velocity, c, is equal in magnitude to the wave velocity of the initial strain attained during impact loading. However, the additional strain computed from these equations is much less than the difference between the measured and computed plastic strain. As an example, for a maximum strain of 4 per cent, the variation of stress in the stress-time record is less than 200 lb/in.^{2} hence, $\Delta\sigma_1 \leq$ 200 lb/in.^{2} The propagation velocity of a plastic strain of 4 per cent magnitude is equal to, $c = 2.12 \times 10^4$ in./sec, and the computed increment of strain, $\Delta\varepsilon_2$, is equal to 0.03 per cent. The difference between the measured and calculated maximum plastic strain from the stress-strain relation at this same value is equal to 0.3 per cent. Thus, the maximum additional strain which can be attributed to relaxation is only one-tenth of the difference between the measured and computed values, or less than 1 per cent of the final strain.

It is seen from equations (8) and (9) that if the velocity of propagation, c, is decreased, the value of $\Delta\varepsilon_2$, increases. The value of c which satisfies the values of $\Delta\sigma_1 = 200$ lb/in.^{2} and $\Delta\varepsilon_2 = 0.3$ per cent can be determined from the equations. The wave velocity for these conditions is computed to be equal to 1900 in./sec. This indicates that the additional strain is propagated through the specimen with a velocity less than one-tenth of the propagation velocity of the initial strain, and hence the distance of propagation of this strain is much less than the distance propagated by the initial strain. This is in contrast with the measured plastic strain distributions, since a region of uniform strain exists near the impact end of the specimen. Therefore, the discrepancy between the stress-strain relations deduced from stress-velocity measurements and the relation determined from stress-plastic strain measurements cannot be attributed primarily to strain relaxation.

It is possible that a single stress-strain relation which describes the behavior of the material for all impact velocities does not exist. A family of stress-strain relations which depend upon the velocity of impact or final strain during impact might explain the discrepancy between measured strain values and the values deduced from stress-velocity measurements. This can be seen from the stress-strain relations shown in

Fig. 22. The stress-strain curve deduced from stress-velocity measurements is represented by the curve designated (σ - v) in Fig. 22. If the stress-strain relation during loading follows this curve up to the point P, the strain at P is less than the measured value of strain at P'. The stress-strain curve obtained from stress-plastic strain measurements is represented by the curve (σ - ε_p) in Fig. 22. If the stress-strain relation during loading follows this curve up to the point P', the particle velocity computed from this curve is greater than the particle velocity determined from velocity measurements. However, a stress-strain relation can exist, represented by the dashed curve in Fig. 22, such that the stress, strain, and particle velocity computed up to P' are equal to the measured values. This curve is not unique since only the end conditions at P' and the particle velocity computed up to P' are given. Thus, it is evident that the form of the relation must be chosen somewhat arbitrarily in order to qualitatively represent the family of stress-strain curves which depend upon the final value of strain. This form is chosen in the following manner.

If the stress-strain relation during impact follows the stress-strain curve represented by the dashed curve in Fig. 22, the stress and particle velocity up to a given strain, ε, are given by

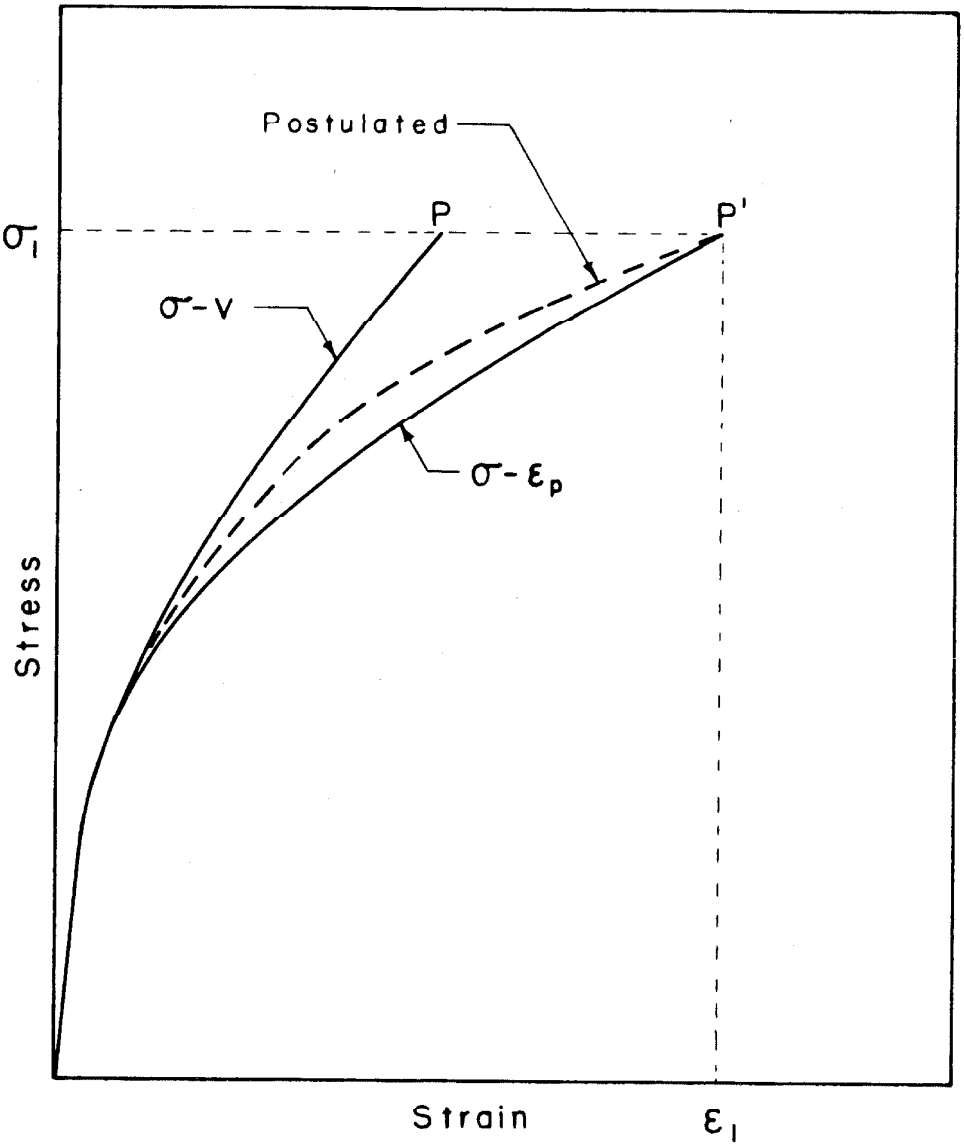

Fig. 22 Three Possible Dynamic Stress-Strain Curves

$$\sigma = \int_0^{\varepsilon} \rho \, c^{*2} \, d\varepsilon \tag{10}$$

$$v = \int_0^{\varepsilon} c^* \, d\varepsilon \tag{11}$$

where c^* is the velocity of propagation for a given strain. Thus, the stress and particle velocity can be expressed in terms of the propagation velocity which is a function of the strain. The propagation velocity, c^*, is defined as

$$\begin{aligned} c^* &= c_o & \varepsilon &= \varepsilon_o \\ c^* &= c + \Delta c & \varepsilon_1 &> \varepsilon > \varepsilon_o \end{aligned} \tag{12}$$

where ε_o is the proportional limit for the particular stress-strain relation,

c_o is the elastic wave velocity,

c is the wave velocity for the corresponding strain on the curve determined from stress-plastic strain measurements,

and Δc is a term which modifies the wave velocity, c.

It is now assumed that the term, Δc, is given by

$$\Delta c = a(\varepsilon - \varepsilon_o) \tag{13}$$

where the values of a and ε_o depend upon the final strain, ε_1. The values of a and ε_o can be determined from equations (10) and (11) since the integrals evaluated at the final strain, ε_1, must be compatible with the measured values of σ and v.

A trail and error solution was used to determine the values of a and ε_o corresponding to a final strain of 2.0, 3.5, and 5.0 per cent. The stress-strain relations corresponding to these values are determined from equation (10). These relations are shown in Fig. 23 by the solid curves. The stress-strain relation determined from stress-plastic strain measurements and the relation deduced from stress-velocity measurements are shown for comparison.

The results indicate that if the stress-strain relation depends upon the final strain during impact, the slope of this curve at the final strain is less than the slope of the curve determined from stress-velocity measurements. This decreased slope corresponds to a lower wave velocity for the final strain. A comparison was made between measured plastic strain distributions and strain distributions deduced from stress-velocity measurements. The comparison indicates that the maximum plastic strain propagates a distance which is less than the computed distance. Since a different stress-strain curve must be used for each final strain or impact velocity, a single Lagrange diagram cannot

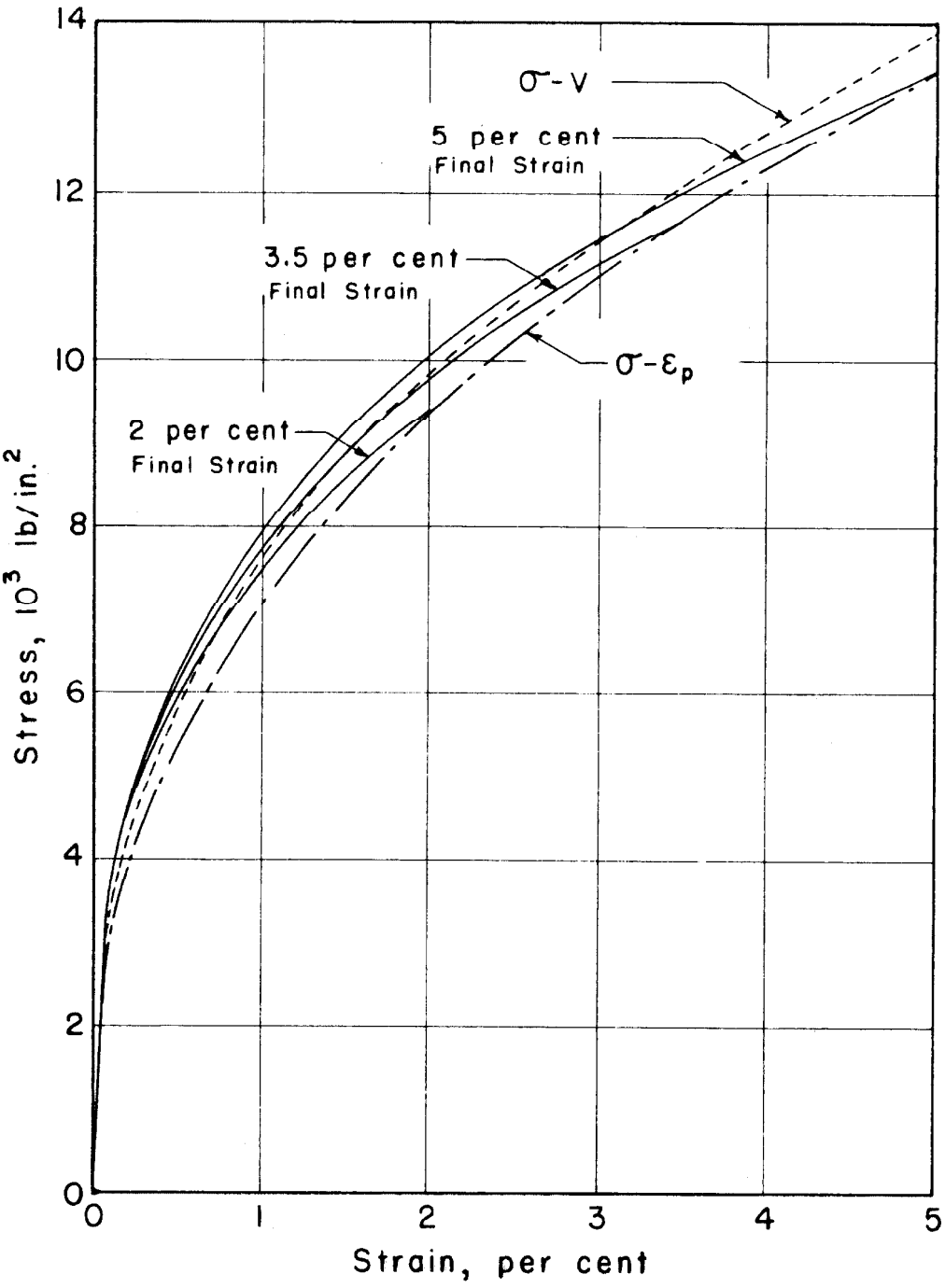

Fig. 23 Derived Dynamic Stress-Strain Curves Which Depend upon the Final Strain in Relation to Curves Based on σ - v and σ - ε_p Measurements

describe the behavior of the material for all impact velocities. In order to compare the distance of propagation of the maximum strain as computed from the stress-strain relations which depend upon the final strain with the measured distance, a Lagrange diagram was constructed from each of the three stress-strain relations determined above. Only the particular section of the Lagrange diagram which determines the final strain propagation distance was constructed. One of these sections for a final strain value of 5.0 per cent is shown in Fig. 24. The results for the three final strain values are presented in Table III. The distances deduced from stress-velocity measurements and the distances from the measured plastic strain distributions are also given for comparison. The results show that the distances computed from the stress-strain relations which depend upon the final strain compare more favorably with the measured values than the distances computed from stress-velocity measurements.

The stress-strain relations which depend upon the final strain, shown in Fig. 23, are consistent in that the curves lie progressively higher for increasing final strains. These curves are similar to curves obtained under increasing rates of loading. If the impact ends of the specimen and anvil bar were plane surfaces, the rate of loading at the impact end of the specimen would be infinite. However, the

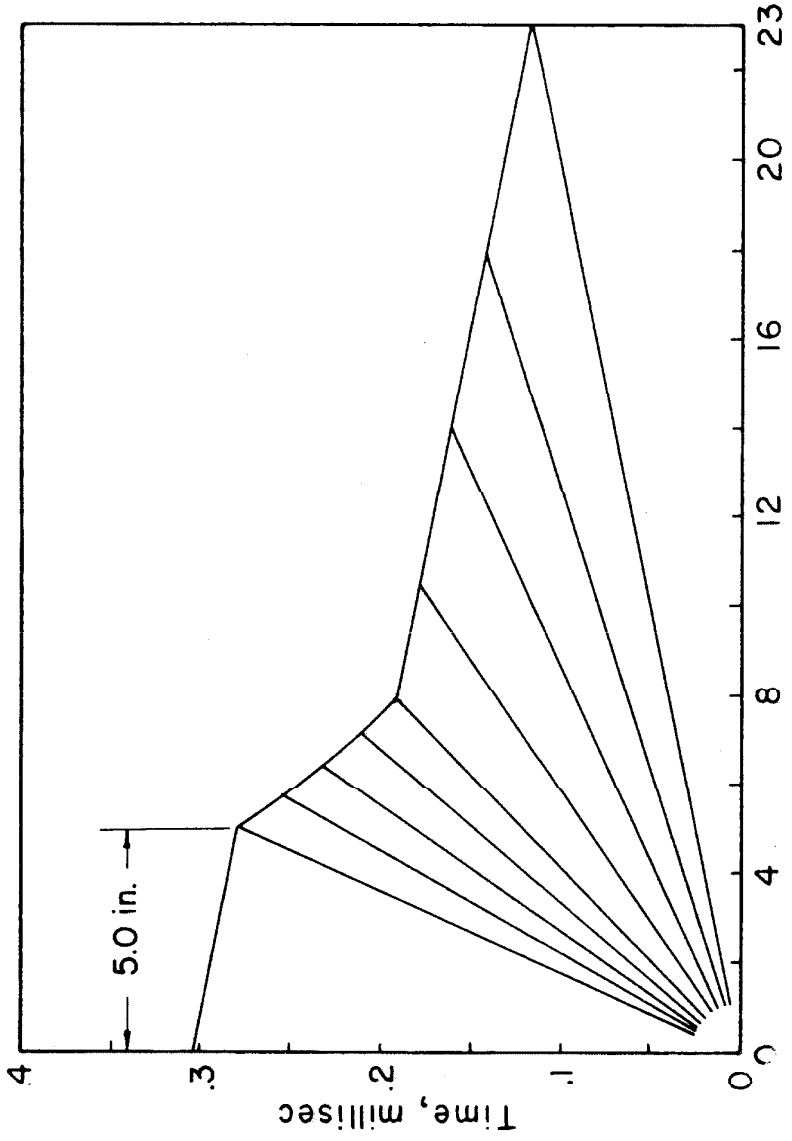

Fig. 24 Lagrange Diagram for Stress-Strain Relation up to 5 Per Cent Strain.

TABLE III

PROPAGATION DISTANCES OF MAXIMUM STRAINS

Maximum Strain per cent	From Plastic Strain Distribution Measurements In.	A In.	B In.
2.0	5.0	7.0	5.9
3.5	4.0	6.2	5.3
5.0	5.0	5.8	5.0

A - From Lagrange diagram deduced from stress-velocity measurements.

B - From Lagrange diagrams deduced from stress-strain relations which depend upon the final strain, ϵ_1.

impact end of the anvil bar used in this investigation is provided with a convex spherical surface. The rate of loading at the impact end of the specimen is equal to a finite value. Since the stress-time records indicate that the rise time of the stress at the interface is less than the 30 microsec rise time of the recording system, the stress rise time cannot be determined from the experimental records. In spite of this, an upper and lower limit on the stress rise time can be determined in the following manner.

If the specimen behaves elastically during impact loading, the stress rise can be determined by a theory developed by Sears (20). As an example, at an impact velocity of 60 ft/sec the time required for the stress to reach a value equal to 95 per cent of the maximum stress is about 7 microsec. If the specimen behaves plastically during impact, the stress rise time is equal to the time required for the plane surface of the specimen end to deform plastically to the spherical surface of the anvil bar end. This time is assumed to be equal to the height of the spherical surface divided by the impact velocity. For an impact velocity of 60 ft/sec, this time is equal to about 2.3 microsec. Thus, the stress rise time for an elastic-plastic specimen is between 2.3 and 7 microsec for an impact velocity of 60 ft/sec. The loading rate increases as the velocity of impact increases

for two reasons. First, the behavior of the material at larger plastic strains or impact velocities is more nearly described by the behavior of a plastic material; and, consequently the rise time of the stress approaches the lower limit of rise time. Second, since the value of the final stress increases, the loading rate increases. This loading rate cannot be applied to the remainder of the impact specimen since the stress, strain, and strain-rate are not uniform along the specimen length. In order to properly describe the behavior during impact of a specimen which exhibits a strain-rate effect, the stress-strain relation must have a time dependence.

An extension of the theory of wave propagation to a material exhibiting a strain-rate effect has been made by Malvern (21). A flow law of the form

$$E_0 \dot{\varepsilon} = \dot{\sigma} + g(\sigma, \varepsilon)$$

was assumed to apply when plastic deformation occurs. The complication introduced by the strain-rate effect in the solution of the problem necessitated the choice of an idealized form of $g(\sigma, \varepsilon)$. Although the theory accounted for several discrepancies observed in the experimental results of previous investigations (5-6), it failed to predict a

region of constant strain near the impact end of the specimen. It seems probable from the experimental results of the present investigation that a simple form of $g(\sigma, \varepsilon)$ cannot describe the behavior of the material under impact loading.

Tests in which the wave velocity is measured as a function of strain offer a means for determining the stress-strain relation up to a strain of 2 per cent during impact loading. The strain in the specimen can be measured as a function of time at two positions along the specimen length with the use of SR-4 strain gages. The time required for a given strain to propagate the known distance between the gages could then be determined from the strain-time records. The velocity of propagation of this strain is equal to the distance between the gages divided by the required time of travel. The stress-strain relation is then determined from the wave velocity-strain relation. This method could not be used in this investigation because the rise time of the recording system is of the same order as the time required for the strains to propagate the distance between the gages.

However, if a recording system of much shorter rise time is employed to determine the wave velocity as a function of the strain, the determinations are limited for the following reasons. The time for an elastic wave to travel a distance equal to the gage length of a SR-4 wire resistance strain gage (1/8 in.) is 0.6 microsec. The time required

for a strain of 2 per cent magnitude to travel the same distance is equal to 5.0 microsec. Thus, the accuracy of strain-time measurments is limited by the time required for the strain to travel a distance equal to the gage length.

A further limitation is imposed by the distortion of the wave front by a dispersive process. The dispersion effect in cylindrical bars was studied experimentally by Kipperger (22). Elastic pulses ranging in duration from 5 to 17 microsec were generated by low velocity impacts of small steel balls on the ends of cylindrical bars. It is found that in order for these pulses to be transmitted along the bar without serious distortion by the dispersive process, the pulses should have a duration at least eight times as long as the time required for an elastic wave to travel a distance equal to one bar diameter. Therefore, in order for a wave front to be propagated through the specimen used in the present investigation without distortion by the dispersive process, the rise time should be greater than the time required for an elastic wave to travel a distance equal to four bar diameters, or 10 microsec. This rise time limitation must be considered in the measurement of wave velocity as a function of strain if the rise time of the stress at the impact end of the specimen is less than 10 microsec.

SUMMARY AND CONCLUSIONS

The results of this investigation show that the dynamic stress-strain relation of annealed 2S aluminum under impact conditions lies considerably above the static stress-strain relation. The increase in stress above the static curve increases progressively from zero at the proportional limit strain to about 20 per cent of the static value at 4.5 per cent strain. The raised stress-strain relation observed under impact conditions cannot be induced by moderate rates of loading, and therefore, this increase is directly attributable to very high rates of loading.

It is shown that a single dynamic stress-strain relation cannot properly describe the behavior of the material for all impact velocities. A stress-strain relation which depends upon the final strain is postulated in order to explain the difference between the stress-strain curve deduced from stress-velocity measurements and the curve determined from stress-plastic strain measurements. A different stress-strain relation exists for each specific velocity of impact or final strain. The stress-strain relations consist of a family of stress-strain curves whose terminal points lie on the stress-strain relation represented by stress vs. maximum plastic strain.

Experimental evidence indicates that less than 1 per cent of the final strain can reasonably be attributed to relaxation after the initial impact stress has been reached.

An experimental method is suggested which might aid in determining the stress-strain relation during impact loading and its dependence upon the impact velocity or final strain.

APPENDIX

The present theory of the propagation of longitudinal waves of plastic deformation in long thin bars was developed by von Karman (15-16). The methods of integration and graphical solutions for problems of strain propagation were developed by von Karman, Bohnenblust, Hyers, and Charyk; and presented in restricted reports (17-18). Since these reports are not readily available, although they have been declassified, a summary of the graphical solution used in this investigation will be given.

Let the stress-strain relation for the material be given by a function of the form $\sigma = \sigma(\varepsilon)$ where σ is the stress and ε is the strain. This relation holds for the first deformation of the material beyond the elastic limit. If the load is decreased, the stress and strain decrease according to Hooke's law.

Consider a long bar of the material in which one end of the bar is suddenly put into motion by longitudinal impact. The characteristic parameters which define the state of strain and motion of an element in the bar are the following

$$\varepsilon = \frac{\partial u}{\partial x} = \text{strain}$$

σ = stress

$v = \frac{\partial u}{\partial t}$ = particle velocity

where x is the distance along the bar,

and u is the longitudinal displacement of a cross-section.

The equation of motion of a small element of the rod, neglecting the kinetic energy and shear stresses associated with the radial motion of the bar, is given by

$$\rho \frac{\partial v}{\partial t} = \frac{\partial \sigma}{\partial x}$$

where ρ is the mass density of the material. Using the relation for the velocity of propagation of a plastic strain as shown by von Karman (15),

$$c = \sqrt{\frac{d\sigma}{d\varepsilon}/\rho} ,$$

the equation of motion becomes

$$\frac{\partial v}{\partial t} = c^2 \frac{\partial \varepsilon}{\partial x} . \qquad (14)$$

On the other hand, from the relations $v = \frac{\partial u}{\partial t}$ and $\varepsilon = \frac{\partial u}{\partial x}$ it follows that

$$\frac{\partial v}{\partial x} = \frac{\partial \varepsilon}{\partial t} . \qquad (15)$$

By using a transformation of variables, the strain, ε, and the particle velocity, v, are introduced as independent variables. Then equations (14) and (15) take the form

$$\frac{\partial x}{\partial \varepsilon} = c^2 \frac{\partial t}{\partial v}$$

$$\frac{\partial t}{\partial \varepsilon} = \frac{\partial x}{\partial v} . \tag{16}$$

The equations become more symmetrical by introduction of the function $\phi = \int_0^{\varepsilon} c\,d\varepsilon$. The equations become

$$\frac{\partial x}{\partial \phi} = c \frac{\partial t}{\partial v}$$

$$\frac{\partial x}{\partial v} = c \frac{\partial t}{\partial \phi} . \tag{17}$$

The process of propagation can be represented in a Lagrangean plane with x and t as coordinates, and a velocity plane with v and ϕ as coordinates. The equations (17) have fixed characteristics in the $v\phi$ plane. They are given by the family of straight lines $v - \phi$ = constant and $v + \phi$ = constant. The Lagrange diagram serves as a means of representing the values of stress, particle velocity, and strain at any time and position along the specimen. The details in the construction

of the Lagrange diagram shown in Fig. 10 are given below.

The relations c vs. ϵ, ϕ vs. ϵ, ϕ vs. ϵ, and ϕ vs. σ are plotted from the engineering stress-strain curve of the material. Compression stresses will be taken to be positive and particle velocity will be taken to be positive when the material moves toward the right of the Lagrange diagram shown in Fig. 10. It is assumed that the behavior of the material is characterized by the given stress-strain relation for increasing or constant values of strain and that Hooke's law holds for decreasing strain.

The Lagrange diagram consists of two regions; the plastic region, and the hysteresis region. In the plastic region, the quantity $v + \phi$ is constant along the characteristic of slope $1/c$, while the quantity $v - \phi$ is constant along the characteristic of slope $-1/c$. The plastic region is also described by the differential equations $\frac{\partial \sigma}{\partial x} = -\rho \frac{\partial v}{\partial t}$ and $\frac{\partial \sigma}{\partial t} = -\rho c^2 \frac{\partial v}{\partial x}$. Similarly, in the hysteresis region, the quantity $v + \frac{\sigma}{\rho c_o}$ is constant along the characteristic of slope $1/c_o$ while the quantity $v - \frac{\sigma}{\rho c_o}$ is constant along the characteristic $-1/c_o$. The hysteresis region is also described by the differential equations $\frac{\partial \sigma}{\partial x} = -\rho \frac{\partial v}{\partial t}$ and $\frac{\partial \sigma}{\partial t} = -\rho c_o^2 \frac{\partial v}{\partial x}$. The construction of the Lagrange diagram consists in determining the characteristics in the plastic and hysteresis regions.

The determination of the boundary between the plastic and hysteresis regions allows the characteristics in both regions to be constructed.

The construction of the Lagrange diagram is simplified if it is assumed that the specimen is initially at rest and a moving anvil bar strikes the end of the specimen. At time, $t = 0$, the anvil bar moving with a velocity, V_o, strikes the specimen and a series of plastic strains are propagated toward the free end of the specimen. The particle velocity at the end of the specimen is equal to the value of ϕ corresponding to the stress at the impact end. The values of σ and v are determined from the relation given by equation (4) and the ϕ vs. σ curve. The propagation velocity of the plastic strains vary from c_o for the "elastic front" to c_1 for the "plastic front" where c_1 is determined from the ϕ vs. c curve.

At time, $t = l/c_o$, where l is equal to the specimen length, the elastic wave reaches the free end of the specimen and reflects as an unloading "shock wave". This "shock wave" is stopped at a point, 2, which is determined from the equation

$$\frac{2\sigma_1}{\rho c_o} = v_2 - \frac{\sigma_2}{\rho c_o} \tag{18}$$

where σ_1 is the proportional limit of the material,

σ_2 is the stress at the point 2,

and v_2 is the particle velocity at the point 2.

Since σ and v are known along each characteristic, the point 2 can be readily determined.

The Lagrange diagram now consists of two regions, the plastic region below the unloading wave and the hysteresis region above the unloading wave. The stress and particle velocity are discontinuous across the boundary since the unloading "shock wave" is of finite magnitude. The remaining portion of the boundary between the plastic and hysteresis regions in considerably more complicated than the boundary obtained from the unloading "shock wave". The stress and particle velocity are continuous across the remaining portion of the boundary between the plastic and hysteresis regions, but in general their partial derivatives are not continuous. Using the differential equation of motion and expressing the fact that σ and v are continuous across the boundary, the following equation is obtained

$$\left[2\left(\frac{dx}{dt}\right)^2 - (c^2 + c_o^2)\right]\left[\left(\frac{\partial v}{\partial x}\right)_h - \left(\frac{\partial v}{\partial x}\right)_p\right]$$

$$= (c_o^2 - c^2)\left[\left(\frac{\partial v}{\partial x}\right)_h + \left(\frac{\partial v}{\partial x}\right)_p\right] \qquad (19)$$

where $\left(\frac{\partial v}{\partial x}\right)_h$ denotes the value of the partial derivative on the hysteresis side,

$\left(\frac{\partial v}{\partial x}\right)_p$ denotes the value of the partial derivative on the plastic side,

and $\frac{dx}{dt}$ is the slope of the boundary.

The method of solution of the boundary is dictated by this equation.

In the solution of the boundary on the right side of the Lagrange diagram shown in Fig. 10, the plastic region is to the left of the boundary and the hysteresis region to the right. The boundary is assumed to be constructed up to a cross-section, t = constant, passing through a point F of the boundary (see Fig. 25). A characteristic, α, is chosen arbitrarily in the hysteresis region and the problem is to determine the end point, P, of α where α intersects the plastic region. The boundary is given by the line FP. The plastic and hysteresis regions are then constructed up to the new cross-section passing through P. The unknown point, P, lies in one of five regions. A different method, determined by equation (19), applies in each region, but in all cases the value of $v - \frac{\sigma}{\rho c_o} = k_1$ is known along the characteristic α. The five regions in which P may lie are determined by the following conditions.

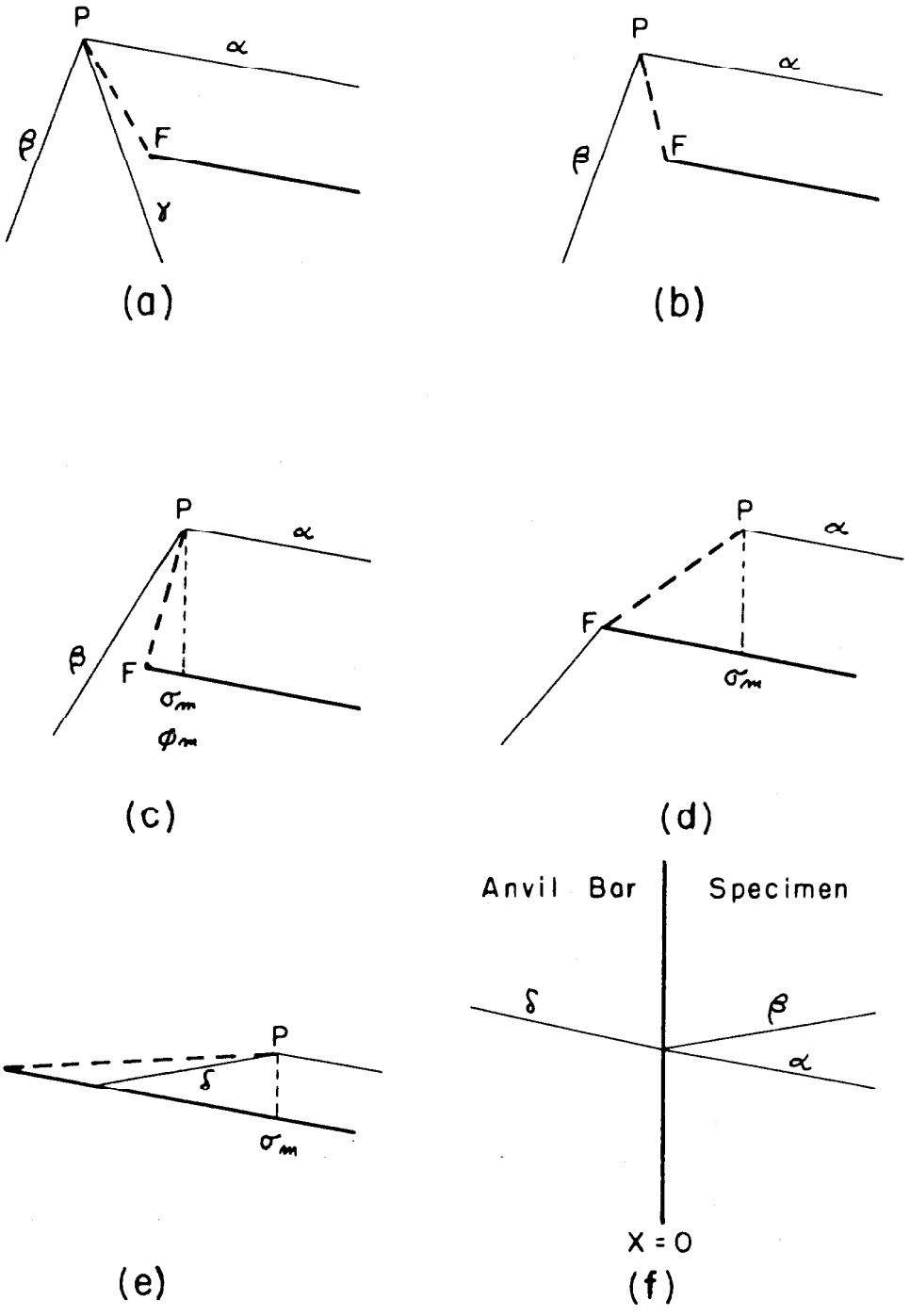

Fig. 25 Steps Illustrating Construction of Lagrange Diagram

Region A (Fig. 25 a) $\frac{1}{c} < \frac{\Delta t}{\Delta x} < \frac{-1}{c_o}$

Choose a characteristic α along which $v - \frac{\sigma}{\rho c_o} = k_1$

Along β $\qquad v + \phi = k_2$ (20)

Along γ $\qquad v - \phi = k_3$ (21)

The value of v and ϕ at P can be computed from equations (20) and (21). The value of σ corresponding to ϕ is obtained from the $\sigma - \phi$ curve. These values of v and σ must be compatible with α.

Region B (Fig. 25 b) $\frac{\Delta t}{\Delta x} < -\frac{1}{c}$

In this case, $\frac{\partial \sigma}{\partial t} = \frac{\partial v}{\partial x} = 0$ along the boundary from equation (19). This implies that $\frac{\sigma}{\rho c_o} + \frac{v}{c_o}\left(\frac{dx}{dt}\right)$ is constant along the boundary and therefore equal to its value at F.

Choose a characteristic α along which $v - \frac{\sigma}{\rho c_o} = k_1$.

Along the boundary $\frac{\sigma}{\rho c_o} + \frac{v}{c_o}\left(\frac{dx}{dt}\right) = k_3$ (22)

Along β $\qquad v + \phi = k_2$ (23)

The constant value of $v + \phi = k_2$ along the characteristic of slope 1/c which abuts at P must be compatible with α and equation (22).

Region C (Fig. 25 c) $\frac{\Delta t}{\Delta x} > \frac{1}{c}$

Choose a characteristic α along which $v - \frac{\sigma}{\rho c_o} = k_1$.

Along β $\qquad v + \phi = k_2 \qquad (24)$

At P, $\sigma = \sigma_{max}$ and $\phi = \phi_{max}$ determined from the previous boundary. The point P is determined from

$$\frac{\sigma_{max}}{\rho c_o} + \phi_{max} = k_2 - k_1.$$

Region D (Fig. 25 d) $1/c_o < \frac{\Delta t}{\Delta x} < \frac{1}{c}$

In this case $\frac{\partial \sigma}{\partial t} = \frac{\partial v}{\partial x} = 0$ along the boundary from equation (19). This implies that $\frac{\sigma}{\rho c_o} + \frac{v}{c_o}\left(\frac{dx}{dt}\right)$ is constant along the boundary and therefore equal to its value at F.

Choose a characteristic α along which $v - \frac{\sigma}{\rho c_o} = k_1$

Along the boundary $\frac{\sigma}{\rho c_o} + \frac{v}{c_o}\left(\frac{dx}{dt}\right) = k_3 \qquad (25)$

At P $\qquad \sigma = \sigma_{max}$.

The value of σ_{max} at P must be compatible with α and equation (25).

Region E (Fig. 25 e)

Choose a characteristic α along which $v - \frac{\sigma}{\rho c_o} = k_1$.

Along δ $$v + \frac{\sigma}{\rho c_o} = k_4 \qquad (26)$$

At P $$\sigma = \sigma_{max}.$$

The following relation must hold

$$\frac{2\sigma_{max}}{\rho c_o} = k_2 - k_1$$

Finally, having found point, P, the Lagrange diagram is extended up to the line, t = constant, passing through P. At P, σ, v, and β have been determined. The values of $v \pm \beta$ and $v \pm \frac{\sigma}{\rho c_o}$ are known along the characteristics starting from P with the slopes $\pm 1/c$ and $\pm 1/c_o$ respectively. The characteristics are then plotted in the plastic and hysteresis regions.

The boundary on the left side of the Lagrange diagram shown in Fig. 10 is constructed in a similar manner. In this case, the plastic region is to the right of the boundary and the hysteresis region to the left of the boundary. A condition equivalent to Region A for the right boundary is used to determine the left boundary.

The hysteresis region on the left side of the Lagrange diagram is extended to the interface, x = 0 and an additional computation must be made to determine the characteristics in the anvil bar and specimen. The characteristics shown in Fig. 25f satisfy the following conditions:

Along α $$v - \frac{\sigma}{\rho c_o} = k_1 \tag{27}$$

Along β $$v + \frac{\sigma}{\rho c_o} = k_2 \tag{28}$$

Along δ $$v - \frac{\sigma}{\overline{\rho c_o}} = k_3 \tag{29}$$

where $\overline{\rho c_o}$ is the acoustic impedance of the anvil bar, and ρc_o is the acoustic impedance of the specimen.

In all cases, the value of $v - \frac{\sigma}{\rho c_o} = k_1$, is known along the characteristic α. Since the anvil bar remains elastic, k_3, is given by

$$k_3 = 2v - V_o \tag{30}$$

where V_o is the velocity of impact. The value of k_2 is determined from equations (27), (28), (29), and (30) giving

$$k_2 = \frac{2V_o \gamma}{\gamma + 1} - k_1 \left(\frac{\gamma - 1}{\gamma + 1} \right) \tag{31}$$

where γ is equal to $\frac{\overline{\rho c_o}}{\rho c_o}$. The stress and particle velocity at the interface are given by

$$\sigma = \frac{(k_2 - k_1)}{2} \rho c_o \tag{32}$$

$$v = \frac{k_1 + k_2}{2} \tag{33}$$

The values of σ, v, and ϕ are tabulated for each characteristic intersection and determined boundary point. The values between these intersections and points are determined by linear interpolation. Thus, the values of σ, v, and ϕ for any time or position along the specimen can be determined directly from the Lagrange diagram.

The plastic strain distribution in the specimen after impact is obtained from the Lagrange diagram. The highest value of ϕ reached at various positions along the bar are determined at the plastic-hysteresis boundary, and translated into ε values from the $\phi - \varepsilon$ curve. The strains are then corrected for elastic recovery upon removal of load.

The strain-time relation at any position along the specimen is similarly obtained from the Lagrange diagram. The values of ε along a line, x = constant, are determined by reading from the $\phi - \varepsilon$ curve, the values of ε corresponding to the values of ϕ.

The stress-time relation at the interface between the anvil bar and specimen is determined from the Lagrange diagram along the line, x = 0.

REFERENCES

(1) H. C. Mann, "High Velocity Tension Impact Tests," Proceedings, Am. Soc. Testing Mats. (1936), Vol. 36, Part II, p. 85.

(2) D. S. Clark and G. Datwyler, "Stress-Strain Relations under Tension Impact Loading," Proceedings, Am. Soc. Testing Mats. (1938), Vol. 38, Part II, p. 98.

(3) M. Manjoine and A. Nadai, "High Speed Tension Tests at Elevated Temperatures," Proceedings, Am. Soc. Testing Mats. (1940), Vol. 40, p. 822; Transactions, Am. Soc. Mechanical Engrs., Journal of App. Mech. (1941), Vol. 8, No. 2, p. A-77.

(4) D. S. Clark, "The Influence of Impact Velocity on the Tensile Characteristics of Some Aircraft Metals and Alloys," Nat. Advisory Comm. Aeronautics (October, 1942) Technical Note No. 868.

(5) P. E. Duwez and D. S. Clark, "An Experimental Study of the Propagation of Plastic Deformation under Conditions of Longitudinal Impact," Proceedings, Am. Soc. Testing Mats. (1947), Vol. 47, p. 502.

REFERENCES

(6) D. S. Clark and P. E. Duwez, "Discussion of the Forces Acting in Tension Impact Tests of Materials," Transactions, Am. Soc. Mechanical Engrs., Journal of App. Mech. (1948), Vol. 15, No. 3, p. A-243.

(7) G. I. Taylor, "The Use of Flat Ended Projectiles for Determining Dynamic Yield Stress, Part I," Proceedings, Royal Society (1948), 194, 1038, p. 289.

(8) A. C. Whiffin, "The Use of Flat Ended Projectiles for Determining Dynamic Yield Stress, Part II," Proceedings, Royal Society (1948), 194, 1038, p. 299.

(9) E. T. Habib, "A Method of Making High-Speed Compression Tests on Small Copper Cylinders," Journal of App. Mech., Transactions, Am. Soc. Mechanical Engrs., Vol. 70, (1948) p. 248.

(10) D. S. Wood and D. S. Clark, "The Tensile Impact Properties of Some Metals and Alloys," Transactions, Am. Soc. for Metals (1950), Vol 42, p. 45.

(11) E. H. Lee and H. Wolf, "Plastic-Wave Propagation Effects in High-Speed Testing," Journal of App. Mech. (1951), Vol. 18, No. 4, p. 379.

REFERENCES

(12) D. S. Clark and D. S. Wood, "The Time Delay for the Initiation of Plastic Deformation at Rapidly Applied Constant Stress," Proceedings, Am. Soc. Testing Mats. (1949), Vol. 49, p. 77.

(13) J. E. Johnson, D. S. Wood, and D. S. Clark, "Delayed Yielding in Annealed Low Carbon Steel under Compression Impact," Fifth Technical Report submitted to the Office of Naval Research, March 1952.

(14) H. Kolsky, "An Investigation of the Mechanical Properties of Materials at Very High Rates of Loading," Proceedings, Physical Soc. London (1949), Vol. 62, p. 176.

(15) Th. von Karman, "On the Propagation of Plastic Deformation in Solids," NDRC Report No. A-29 (OSRD No. 365), (1942).

(16) Th. von Karman and P. E. Duwez, "The Propagation of Plastic Deformation in Solids," Journal of Applied Physics (1950), Vol. 21, No. 10, p. 987.

(17) Th. von Karman, H. F. Bohnenblust, and D. H. Myers, "The Propagation of Plastic Waves in Tension Specimens of Finite Length, Theory and Methods of Integration," NDRC Report No. A-103, (OSRD No. 946), August 1942.

(18) H. F. Bohnenblust, J. V. Charyk, and D. H. Myers, "Graphical Solutions for Problems of Strain Propagation

REFERENCES

in Tension," NDTC Report No. A-131, (OSRD No. 1204), December, 1942.

(19) E. Jones and K. R. Maslan, "The Physical Characteristics of Wire Resistance Strain Gages," Royal Aircraft Establishment, Farnborough, England.

(20) J. E. Sears, "On the Longitudinal Impact of Metal Rods with Rounded Ends," Transactions, Cambridge Philosophical Soc., Vol. 21, No. 2, p. 49.

(21) L. E. Malvern, "The Propagation of Longitudinal Waves of Plastic Deformation in a Bar of Material Exhibiting a Strain-Rate Effect," Journal of App. Mech. (1951), Vol. 18, No. 2, p. 203.

(22) E. A. Ripperger, "The Propagation of Pulses in Cylindrical Bars," Stanford University, Division of Engr. Mech., Navy Contract N6-ONR-251, Tech. Report No. 13, (1952).